CANCER

Desmosomal proteins of DSC2 and PKP1 promote cancer cells survival and metastasis by increasing cluster formation in circulatory system

Koukou Li[1], Renfei Wu[1], Muya Zhou[1], Haibo Tong[1], Kathy Q. Luo[1,2]*

To study how cancer cells can withstand fluid shear stress (SS), we isolated SS-resistant breast and lung cancer cells using a microfluidic circulatory system. These SS-resistant cells showed higher abilities to form clusters, survive in circulation, and metastasize in mice. These SS-resistant cells expressed 4.2- to 5.3-fold more desmocollin-2 (DSC2) and plakophilin-1 (PKP1) proteins. The high expression of DSC2 and PKP1 facilitated cancer cells to form clusters in circulation, and also activated PI3K/AKT/Bcl-2–mediated pathway to increase cell survival. The high levels of DSC2 and PKP1 are also important for maintaining high expression of vimentin, which stimulates fibronectin/integrin β_1/FAK/Src/MEK/ERK/ZEB1–mediated metastasis. Moreover, higher levels of DSC2 and PKP1 were detected in tumor samples from patients with breast and lung cancer, and their high expression was correlated with lower overall survival and worse disease progression. DSC2 and PKP1 may serve as new biomarkers for detecting and targeting metastatic circulating tumor cells.

INTRODUCTION

Circulating tumor cells (CTCs) are the major source of metastatic tumors, which cause 90% of cancer-associated deaths (*1*, *2*). Although millions of cancer cells can be shed from the primary tumor, most of them die in circulation, whereas few CTCs (<0.02%) can eventually colonize at distant organs (*1*, *3*–*5*). Thus, understanding how these special CTCs can survive in circulation and form metastatic tumors is crucial for designing new therapies to prevent metastasis and increase the survival of patients with cancer.

When cancer cells cross the monolayer of endothelial cells and enter the circulatory system, they will encounter four challenges: hemodynamic shear stress (SS), anoikis (apoptosis caused by the lack of adhesion), immunosurveillance mediated mainly by nature killer (NK) cells and cytotoxic T cells, and collisions with blood cells and vascular endothelial cells (*6*–*10*). CTCs must overcome all these challenges, especially hemodynamic SS, to survive in circulation (*11*).

The levels of SS in human blood flow vary greatly, ranging from 0.5 to 4 dynes/cm^2 in the veins, 4 to 30 dynes/cm^2 in the arteries, and above 60 dynes/cm^2 in the vascular system near the heart (*12*, *13*). These different levels of SS can produce very different effects when they are imposed on CTCs. For example, lower levels of SS (<5 dynes/cm^2) did not harm the cells and actually stimulated cell migration (*14*–*16*). In contrast, arteriosus levels of SS (12 to 30 dynes/cm^2) significantly increased the apoptotic rate and reduced cell viability (*15*, *17*, *18*). Further elevation of SS to 60 dynes/cm^2 or higher levels destroyed the cells via necrosis (*17*) or fragmentation (*10*, *19*). Hence, arteriosus SS not only destroys CTCs in circulation but also reduces their metastatic capabilities (*20*, *21*).

To withstand the damaging effects of SS, CTCs have developed various survival mechanisms. For example, it has been proposed that epithelial-mesenchymal transition (EMT) may promote CTCs' survival and early colonization (*22*). CTCs from patients with cancer have shown elevated expression of twist (EMT marker), epidermal growth factor receptor (EGFR), human EGFR 2 (HER2), HER3, hepatocyte growth factor receptor (MET), phosphoinositide 3-kinase (PI3K), and Akt, suggesting a link between EMT and activation of the PI3K-Akt survival pathways in CTCs (*23*–*25*). High expression of the RhoA–myosin II axis, lamin A/C, or the small guanosine triphosphatase Rac1 helped CTCs acquire more resistance to SS-induced membrane and nuclear damage (*10*, *26*–*28*). Elevated activation of oncogenic signaling molecules such as Ras, Myc, and PI3K also contributed to cellular resistance to fluidic SS (*10*, *16*, *29*, *30*). Moreover, higher expression of β-globin or manganese superoxide dismutase protected CTCs from the damaging effects of SS-induced reactive oxygen species (*15*, *31*).

In addition, CTCs may use other strategies, such as forming clusters, to resist shear forces. For example, it has been reported that when tumor cell aggregates containing more than two CTCs (defined as CTC clusters) were intravenously injected into mice, these CTC clusters had a higher metastatic potential than single CTCs of melanoma or lung cancer (*29*, *32*). Aceto *et al.* (*33*) also found that CTC clusters (2 to 5% of all CTCs) displayed 23 to 50 times higher metastatic potential than single CTCs and those CTCs expressed higher levels of plakoglobin (PG). Moreover, the number of CTC clusters was higher in patients with recurrent breast cancer or in patients who developed drug resistance (*30*, *33*). Last, Liu *et al.* (*34*) reported that homophilic CD44 interactions mediate tumor cell aggregation and polyclonal metastasis in patient-derived breast cancer models.

Most of the known survival mechanisms of CTCs were obtained from single CTCs or from a total population of CTCs, while fewer reports have focused on the mechanisms and pathways used for CTCs to survive as clusters. In this study, we used a microfluidic circulatory system to select cancer cells that could survive multiple rounds of SS treatment, most of which existed in clusters. By characterizing these SS-resistant and cluster-enriched cells, we identified the molecular basis of cluster formation and elucidated the underlying mechanisms through which clustered cancer cells survived in circulation and formed metastatic colonies in lung tissues.

[1]Faculty of Health Sciences, University of Macau, Taipa, Macao SAR, China. [2]Ministry of Education Frontiers Science Center for Precision Oncology, University of Macau, Taipa, Macao SAR, China.
*Corresponding author. Email: kluo@um.edu.mo

RESULTS

Clustered cancer cells are more resistant to cell death than single cells in circulation

In our previous study, we developed a microfluidic circulatory system that used a peristaltic pump to drive the injected cancer cells to circulate in a 1.5-m-long tube that was precoated with 1% Pluronic F-127 to prevent cell attachment (fig. S1A) (*15*, *17*, *35*). In this study, to determine the effects of different levels of SS on cancer cell viability, we set the flow rates of the circulatory system to produce one venous level of SS at 5 dynes/cm^2 (SS5) and two arteriosus levels of SS at 15 dynes/cm^2 (SS15) and SS at 20 dynes/cm^2 (SS20). MCF7-C3 cells expressing apoptotic sensor proteins were circulated under these three levels of SS for 12 hours, and cell viability was determined by the 3-(4,5-dimethylthiazol-2-yl)-2,5-diphenyltetrazolium bromide (MTT) assay. The results showed that circulating cancer cells under SS5 did not cause a significant level of cell death, whereas circulating cells under both SS15 and SS20 significantly reduced cell viability from 96 to 19 and 12%, respectively (Fig. 1A). Although SS20 further reduced cell viability, there was no significant difference between the viabilities of SS15 and SS20 (Fig. 1A). We thus selected SS15, which also represents the average SS present in a human artery (*10*), as the level of SS to circulate cancer cells in this study.

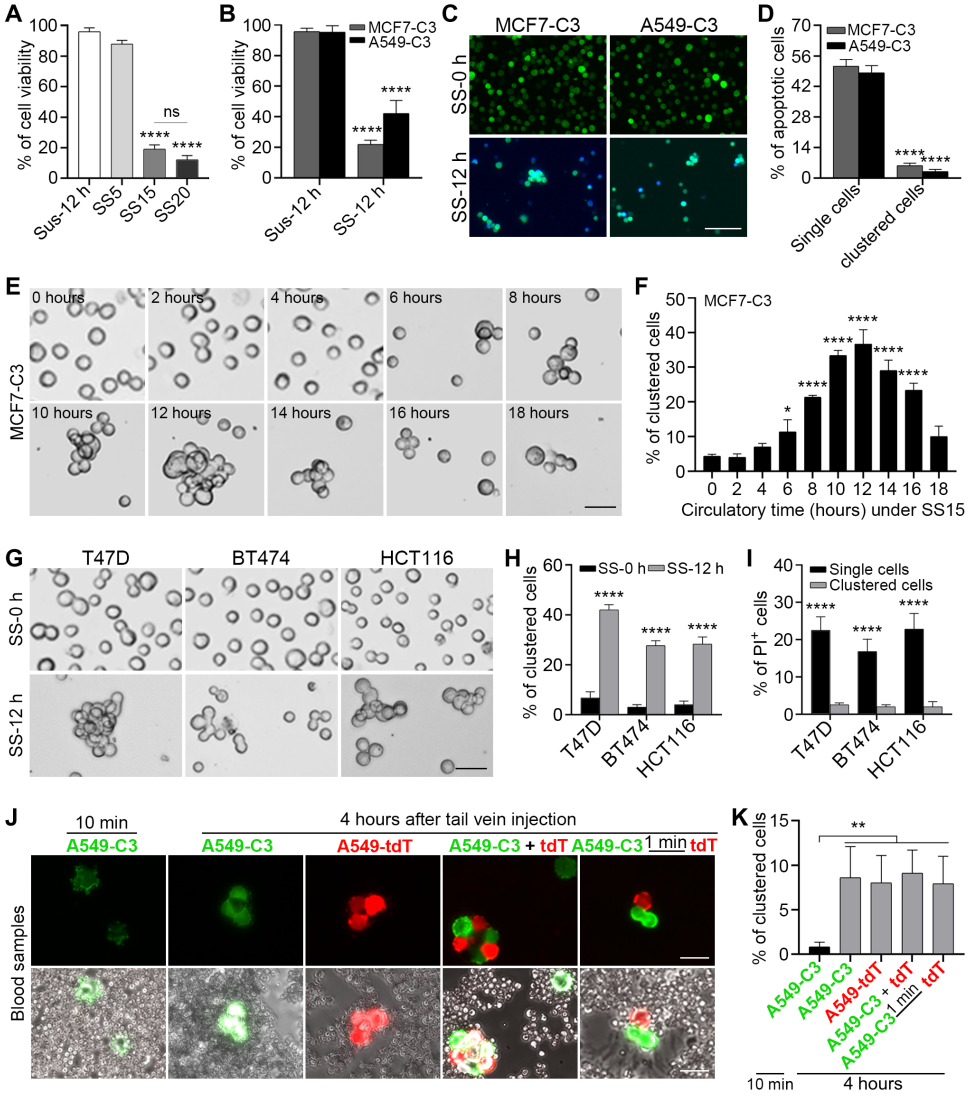

Fig. 1. Clustered cells were more resistant to SS-induced cell death than single cells. (**A** and **B**) MTT assays were used to determine the viabilities of MCF7-C3 (A) or MCF7-C3 and A549-C3 cells (B) under indicated conditions. (**C** and **D**) Fluorescence resonance energy transfer (FRET) images analysis was used to indicate (green live cells and blue apoptotic cells) (C) and quantify apoptotic rates in single and clustered cells (D) (cell numbers, ≥300). Scale bar, 100 μm. (**E** and **F**) Phase images (E) and quantified percentage of clustered MCF7-C3 cells (F) under SS15 for 0 to 18 hours. Scale bar, 50 μm. (**G** and **H**) Phase images (G) and quantified percentage of clustered cells of indicated cell lines (H) under SS15 for 0 and 12 hours (cell numbers, ≥300). Scale bar, 50 μm. (**I**) Quantified percentage of propidium iodine–positive (PI$^+$) cells under indicated conditions (cell numbers, ≥300). (**J** and **K**) A549-C3 or A549-tdTomato (A549-tdT) cells were injected into the tail vein of nonobese diabetic/severe combined immunodeficient (NOD/SCID) mice (n = 5 mice per group). Representative images of CTC clusters and blood cells (J) and quantified percentage of CTC clusters (K) from blood smears (cell numbers, ≥200). Scale bars, 25 μm. The quantified results are the average percentage ± SD obtained from three independent experiments. *P < 0.05, **P < 0.01, and ****P < 0.0001. ns, not significant.

To achieve real-time detection of cell death after circulatory treatment, we used two sensor cell lines. These cells change their fluorescence from green to blue when they undergo apoptosis. The MCF7-C3 sensor cell line was generated from MCF7 breast cancer cells, and the A549-C3 sensor cell line was generated from A549 lung cancer cells. The sensor cells were trypsinized into single cells, and 2×10^5 cells in 1 ml of culture medium with 10% fetal bovine serum (FBS) were circulated in each channel of the microfluidic circulatory system under SS15 in a 37°C CO_2 incubator for 12 hours (SS-12 h). To avoid variations between different channels, we combined the cells from at least two channels after the circulatory experiment at the indicated time point. We also left the cells under suspension conditions for 12 hours (Sus-12 h) as a control group. The viability of the cells was determined by the MTT assay. The quantified results showed that although more than 90% of the cells formed large aggregates after being left in the suspension for 12 hours (fig. S1, B and C), 95 to 96% of the MCF7-C3 and A549-C3 cells were viable (Fig. 1B). In contrast, the SS treatment markedly decreased the viability of these cells from 95 to 96% to 22 to 42% (Fig. 1B).

From the fluorescence resonance energy transfer (FRET) images, we observed that some of the cancer cells formed aggregates or clusters after 12 hours of circulatory treatment (Fig. 1C). We then counted the numbers of green live cells and blue apoptotic cells that were in the states of single cells or cluster with ≥3 cells. The quantified results showed that the single MCF7-C3 and A549-C3 cells had much higher percentages of apoptosis (51 and 48%), while the clustered cells had a significantly lower rate of apoptosis (5.1 and 3.2%) (Fig. 1D). These results suggested that clustered cells are more resistant to SS-induced cell death.

Time course analysis of the phase images of MCF7-C3 cells revealed that clusters were formed during circulatory treatment in a time-dependent manner (Fig. 1E). The quantified results showed that the percentages of clustered cells did not increase within the first 4 hours, increased to 11% at 6 hours, reached the highest value of 37% at 12 hours, and declined to 10% at 18 hours (Fig. 1F). Circulating the breast cancer T47D and BT474 cells and the colorectal cancer HCT116 cells under SS15 for 12 hours also resulted in a significant increase in clustered cells from 2.2 to 6.7% to 28 to 42% (Fig. 1, G and H). Similar to the results shown in Fig. 1D, the percentages of propidium iodine (PI)–stained dead cells were also much higher in the single cells (17 to 23%) than in the clustered cells (1.9 to 2.5%) (Fig. 1I and fig. S1D). While leaving cells of T47D, BT474, and HCT116 under suspension conditions for 12 hours resulted more than 90% of the cells to form aggregates, around 95% of the cells were viable (fig. S1, E to G). Together, these results showed that when cancer cells were circulated under an arteriosus SS, they could form clusters, and these clustered cancer cells displayed a higher survival ability than single cancer cells.

To test whether cancer cells can form clusters in vivo, we injected 2 million green fluorescent A549-C3 cells into the tail vein of nonobese diabetic/severe combined immunodeficient (NOD/SCID) mice and collected blood samples at 10 min and 4 hours. The results of microscopy analysis of blood smears revealed that the percentage of clustered cancer cells was significantly increased from 0.8% at 10 min to 8.6% at 4 hours after cell injection, which indicated that individual cancer cells could form clusters in blood circulation (Fig. 1, J and K). We also injected the same numbers of red fluorescent A549-tdTomato (A549-tdT) cells into the tail vein of NOD/SCID mice and a similar 8.0% percentage of clustered cancer cells were found in the blood samples 4 hours after the cell injection (Fig. 1, J and K).

To confirm these results, we mixed and coinjected 1 million green and 1 million red fluorescent A549 cells into the tail vein or sequentially injected into the tail vein at 1-min intervals. The results showed that these two injection methods also resulted in 9.1 and 7.9% clustered cells (Fig. 1, J and K). We also observed that some of the clusters in the coinjection and sequential injection groups had both green- and red-colored cells (Fig. 1J), which suggests that single cancer cells may form clusters while in blood circulation.

SS-resistant SSP6 cells can form more clusters and survive better in the bloodstream of mice than their parental cells

To study why clustered cells can survive better in circulation, we enriched cells that could form clusters and resist the destructive effect of fluid shear force. MCF7-C3 cells were circulated under SS15 for 15 hours and cultured to yield a cell line called MCF7-C3–SSP1 (M-SSP1). Then, the M-SSP1 cells were subjected to five more rounds of circulatory treatments, and the selected cell lines were named M-SSP2 to M-SSP6 (Fig. 2A). We also generated A549-C3–SSP6 (A-SSP6) cells from the parental A549-C3 cells using the same method. Through these six rounds of selections, both M-SSP6 and A-SSP6 cells displayed significantly higher percentages of clustered cells and viabilities and lower rates of apoptosis than SSP1 cells (fig. S2, A to F). They also showed much higher abilities to form clusters, survive, and resist to apoptosis than the parental MCF7-C3 and A549-C3 cells under a circulatory treatment of SS15 for 15 hours (Fig. 2, B to D).

These SS-resistant cells also displayed higher abilities to proliferate in two-dimensional (2D) culture and to resist apoptosis under suspension conditions than their parental cells (fig. S3, A to D). Moreover, A-SSP6 cells showed much higher ability to form big tumor spheres under 3D conditions within 3 weeks than their parental A549 cells (fig. S3, E and F), but no significant difference was observed between M-SSP6 and its parental cell line (fig. S3G).

Next, we compared cluster formation and survival in the bloodstream between SS-resistant SSP6 cells and their parental cells. Two million cells from each cell line were injected into the tail vein of NOD/SCID mice, and whole blood samples were obtained by cardiac puncture 10 min or 4 hours after injection. At least 100 CTCs were counted from each mouse ($n = 5$). At 10 min after cell injection, very low percentages of CTCs formed clusters of the A549-C3 (0.8%) and A-SSP6 cells (1.4%), which were not significantly different (fig. S4, A and B). However, after 4 hours of cell injection into the bloodstream of mice, SS-resistant cells showed significantly higher cluster formation (41 and 29%) than their parental cells (4.9 and 6.3%, respectively) (Fig. 2, E and F, and fig. S5A). Moreover, FRET imaging analysis showed that these SS-resistant cells also had significantly lower percentages of apoptotic cells (2.8 and 5.2%) than their parental cells (21 and 27%, respectively) (Fig. 2, E and G, and fig. S5A).

Furthermore, we have collected the blood samples every week for 4 weeks after orthotopically implanting 3 million of A549-C3 or A-SSP6 cells into the lung of NOD/SCID mice and quantified the number of single and clustered CTCs from the blood samples. We also examined the blood vessels of the animals to count the number of CTCs remained in circulation by fluorescence microscopy. The results showed that the number of CTC clusters in A-SSP6 group was significantly higher than that in A549-C3 group 2 to 4 weeks after cell implantation (Fig. 2, H and I, and fig. S5, B to D). Collectively, both the in vitro and in vivo results showed that these SS-resistant cells were able to form more clusters and better resisted SS-induced cell death in circulation.

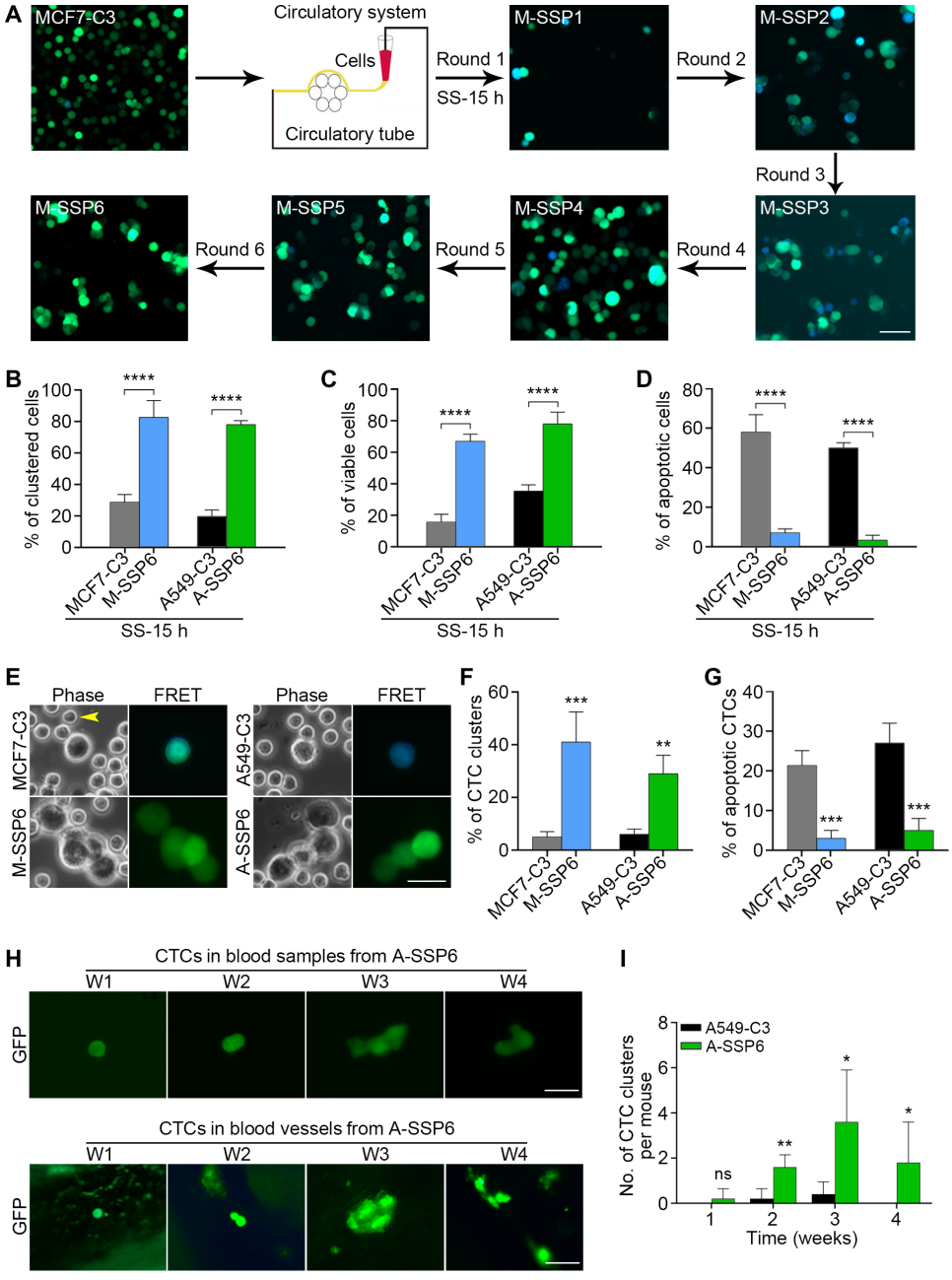

Fig. 2. SS-resistant SSP6 cells displayed higher cluster formation and survival ability than their parental cells. (**A**) FRET images of the selection processes from MCF7-C3 to M-SSP6 cells under SS15 for 15 hours. Scale bar, 100 μm. (**B**) The percentage of clustered cells was quantified by phase microscopy (cell numbers, ≥300). (**C**) The viability was determined by MTT assays. (**D**) The apoptotic rate was determined by FRET imaging analysis (cell numbers, ≥300). (**E** to **G**) SS-resistant and their parental cells were injected into the tail vein of NOD/SCID mice ($n = 5$ mice per group). Four hours later, the phase and FRET images (E) were collected and used to calculate the percentages of clustered CTCs (F) and apoptotic rate (G) (cell numbers, ≥200). Scale bar, 20 μm. The yellow arrowhead indicates blood cells. (**H** and **I**) A549-C3 and A-SSP6 cells were implanted into the lungs of mice, and blood samples were collected. The total number of CTC clusters from blood samples and blood vessels was imaged (H) and calculated (I) weekly for 4 weeks (W) ($n = 5$ mice per group). Scale bars, 25 μm (CTCs in blood samples) and 75 μm (CTCs in blood vessels). The quantified data are the means ± SD from three independent experiments. *$P < 0.05$, **$P < 0.01$, ***$P < 0.001$, and ****$P < 0.0001$.

SS-resistant cells display higher migration, invasion, cell adhesion, colony formation, and metastatic abilities

Three in vitro metastatic assays were used to determine whether SS-resistant cells have higher metastatic capacities than their parental cells. The results showed that both lines of SSP6 cells performed much better than their parental cells in migrating through the Transwell membrane, invading across the Matrigel-coated Transwell membrane and adhering to a monolayer of endothelial cells (Fig. 3, A to D, and fig. S6, A and B). Moreover, the results of colony formation assays showed that both SSP6 cells formed more colonies than their parental cells (Fig. 3E and fig. S6C).

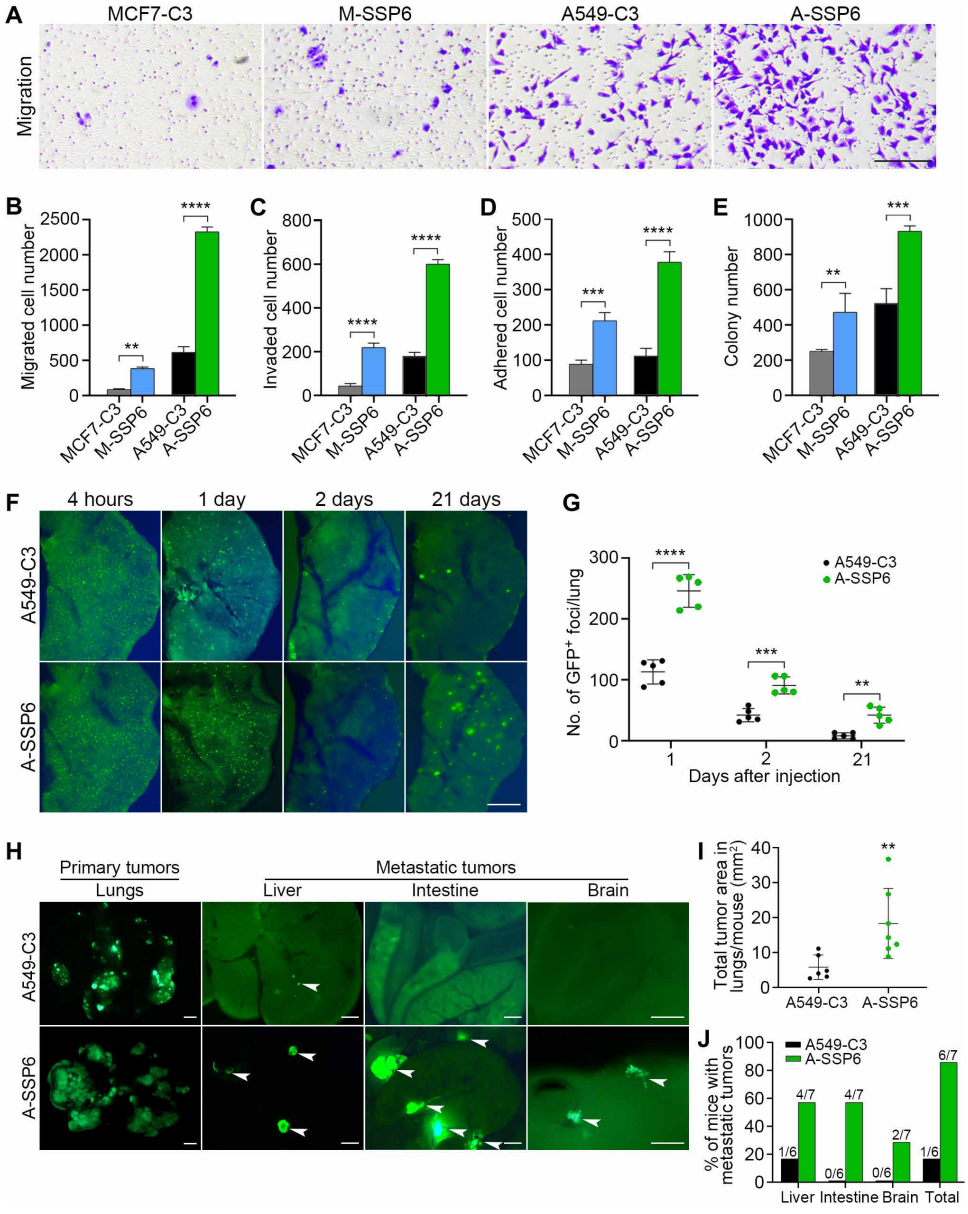

Fig. 3. The SS-resistant SSP6 cells displayed higher metastatic capabilities. (**A** and **B**) Representative images and quantified results of the Transwell migration assays for the MCF7-C3, M-SSP6, A549-C3, and A-SSP6 cells. Scale bar, 200 μm. (**C**) Quantified results of the Transwell invasion assays for the indicated cells. (**D**) Cells attached to the human umbilical vein endothelial cell (HUVEC) monolayer were quantified from five fluorescent images for each cell line. (**E**) Cells were cultured for 10 days and stained with crystal violet for determining the colony numbers. (**F** and **G**) Representative images and quantified numbers of green fluorescent protein–positive (GFP^+) foci per left lung of the mice injected with the A549-C3 and A-SSP6 cells after tail vein injection for 1, 2, and 21 days ($n = 5$ mice per group). Scale bar, 1 mm. (**H**) Representative images of primary tumors formed in the lungs and metastatic tumors in the liver, intestine, and brain in the A549-C3 or A-SSP6 groups. Scale bars, 1 mm (primary lung tumor) and 200 μm (metastatic tumors). White arrowheads indicate metastatic tumors ($n = 6$ to 7 mice per group). (**I**) Quantified total tumor area from the lungs per mouse at 4 weeks after implantation. (**J**) Quantified percentage of mice with metastatic tumors and with metastasis occurring in each group of mice. The results represent the means ± SD. $^{**}P < 0.01$, $^{***}P < 0.001$, and $^{****}P < 0.0001$.

We further examined whether these SS-resistant cells have higher ability to form lung colonies using an experimental lung metastasis model in NOD/SCID mice. One million cells from each cell line were injected into the tail vein of the mice, and fluorescent images of the left side lung were captured at 4 hours and 1, 2, 21, or 30 days after cell injection. The quantified data showed that both SSP6 cell lines resulted in significantly higher numbers of green fluorescent protein–positive (GFP^+) lung foci than their parental cells during both early time points of 1 to 2 days and at the end of the animal experiments. These results indicate that these SS-resistant cells have greatly enhanced abilities to survive in circulation and home to the lung (Fig. 3, F and G, and fig. S6, D, E, and F).

Next, we compared the spontaneous metastatic ability between A549-C3 and A-SSP6 cells by orthotopically implanting 3 million

cells in the right lung of NOD/SCID mice. The body weight of the mice was measured throughout the course of the animal experiments, and there were no differences in the body weight between these two groups (fig. S6G). Four weeks after implantation, the mice were euthanized, and all organs were obtained and examined by fluorescence and phase microscopy. At the primary tumor site in the lung, the quantified results showed that the total tumor area in five pieces of lung tissues per mouse in the A-SSP6 group was 3.1 times larger than that in the A549-C3 group (Fig. 3, H and I).

In terms of metastasis, we observed that among the mice injected with A-SSP6 cells, six of seven mice had large metastatic tumors located in the liver, intestine, and brain. In contrast, for the mice injected with A549-C3 cells, only one of six mice had tiny metastatic tumors in the liver, and no metastatic tumors were found in any other organs (Fig. 3, H and J). These in vitro and in vivo results indicate that these SS-resistant cells also outperformed their parental cells in various aspects of metastasis.

Identification of the key genes that are differentially expressed in the SS-resistant cells

RNA sequencing (RNA-seq) analyses were used to compare the expression profiles between the MCF7-C3 and M-SSP6 cells. The quantified results showed 453 differentially expressed genes ($P < 0.05$) between these two cell lines that are involved in multiple signaling pathways, including cell adhesion, apoptotic process, cell migration, regulation of signaling, cell death, cell proliferation, localization of cell, cytoskeleton, and response to stress (fig. S7, A and B). Under the pathway of cell adhesion, eight genes (fig. S7C) with a 1.5-fold elevation of mRNA levels in the M-SSP6 cells over the MCF7-C3 cells were selected for validation by quantitative reverse transcription polymerase chain reaction (qRT-PCR) in all four cell lines.

The quantified qPCR results showed that among the eight tested genes, desmocollin-2 (DSC2) and plakophilin-1 (PKP1) were expressed at higher levels in both the M-SSP6 and A-SSP6 cells than the parental cells (fig. S7D). We also compared mRNA levels among all 11 desmosomal components, including DSC1 to DSC3, desmogleins (DSG1 to DSG3), PKP1 to PKP3, PG, and desmoplakin (DSP). The results showed that the mRNA levels of DSC2 and PKP1 were higher than the rest of the desmosomal genes in both the M-SSP6 and A-SSP6 cells than their parental cells (fig. S7E). Very high protein levels of DSC2 (4.3- and 5.3-fold) and PKP1 (4.8- and 4.2-fold) were also detected by Western blotting in the M-SSP6 and A-SSP6 cells over their parental cells under normal culture conditions (Fig. 4A).

In addition to DSC2 and PKP1, 11 other proteins involved in cell-cell adhesion were examined. The Western blot results showed that the levels of six proteins, vimentin (VIM), E-cadherin (CDH1), β-catenin, fibronectin (FN1), integrin β_1 (ITGB1), and focal adhesion kinase (FAK), were elevated by 1.9- to 3.8-fold in the M-SSP6 and A-SSP6 cells compared with their parental cells (Fig. 4A). Although the total level of steroid receptor coactivator (Src) did not change significantly, the levels of phosphorylated Src (p-Src) were increased by 2.3- and 1.9-fold in the M-SSP6 and A-SSP6 cells, respectively. One of the desmosomal components, PG, did not change its protein level, and two tight junction proteins, zonula occludens-1 (ZO-1) and claudin-1 (CLDN1), showed significantly reduced levels in the M-SSP6 and A-SSP6 cells (Fig. 4A).

We also determined the mRNA levels of the six genes whose protein levels were elevated in the SSP6 cells (Fig. 4A). The qPCR results showed that for five of the six genes, CDH1, β-catenin, VIM, ITGB1, and FAK, their mRNA levels were significantly increased by 2.1- to 3.3-fold, while no marked increase in FN1 mRNA level was detected between SSP6 and their parental cells (fig. S7F).

We further assessed the distribution of seven up-regulated adhesive proteins by immunofluorescence (IF) staining in the A549-C3 and MCF7-C3 cells before and after the circulatory treatment under SS15 for 12 hours. The fluorescent images showed obvious enhancements at the cell membrane for DSC2, CDH1, β-catenin, and ITGB1 and higher intracellular expression of PKP1, VIM, and FN1 in the A549-C3 and MCF7-C3 cells after SS treatment (Fig. 4B).

As SSP6 cells displayed higher metastatic abilities, we also examined the protein levels of three EMT-related transcription factors, slug, twist, and zinc finger E-box binding homeobox 1 (ZEB1), among which only the protein level of ZEB1 was expressed at higher levels in the SSP6 cells (fig. S7G).

Next, we investigated whether the mRNA levels of some adhesion- and EMT-related genes were changed during the SS treatment. The qRT-PCR results showed that in the A549-C3 cells, the mRNA levels of DSC2, PKP1, VIM, FN1, and ZEB1 were significantly increased during the circulatory treatment under SS15 and reached their highest levels at 8 to 10 hours, while the mRNA level of CDH1 was not significantly changed during the course of the circulatory treatment (Fig. 4C). For the MCF7-C3 cells, the mRNA levels of all six genes were increased during the circulatory treatment and reached their highest levels at various times (fig. S7H). In summary, after RNA-seq and knowledge-based analyses, we identified six candidate genes, DSC2, PKP1, VIM, CDH1, FN1, and ZEB1, whose expressions were elevated after circulatory treatment and in the SS-resistant breast and lung cancer cells.

The dual expression of DSC2 and PKP1 is important for cluster formation and survival in circulation

To determine the importance of these six candidate genes in cluster formation and cell survival, we designed small interfering RNA (siRNA) or short hairpin–mediated RNA (shRNA) to knock down the expression of these genes. Two sets of siRNAs or shRNAs were designed for each of the five target genes, except ZEB1, for which one previously used shRNA in our laboratory was used in this study. The knockdown efficacies of individual siRNAs or shRNAs or different combinations of shDSC2 and shPKP1 were assessed in both SSP6 cell lines by qRT-PCR and Western blotting. The results showed that at least one of the two siRNAs or shRNAs significantly reduced target gene expression at both the mRNA and protein levels in the A-SSP6 cells (fig. S8, A and B) and in the M-SSP6 cells (fig. S9, A and B).

The SSP6 cells were treated with gene-specific siRNA or shRNA and circulated under SS15 for 10 hours. The results showed that knockdown of the expression of DSC2, PKP1, VIM, CDH1, and ZEB1 significantly reduced the cluster formation and survival abilities of SS-resistant A-SSP6 (Fig. 5, A to C, and fig. S10, A to C) and M-SSP6 cells (fig. S10, D to F) under the circulatory treatment of SS15 for 10 hours. However, knocking down FN1 expression did not produce any significant changes in cluster formation or cell survival in A-SSP6 cells (Fig. 5, B and C).

As both DSC2 and PKP1 are components of the desmosome and knocking down PKP1 expression also produced good effects on reducing cluster formation and cell survival under circulatory treatment, we decided to knock down both DSC2 and PKP1. As each gene had two shRNAs, we compared the silencing effects among the

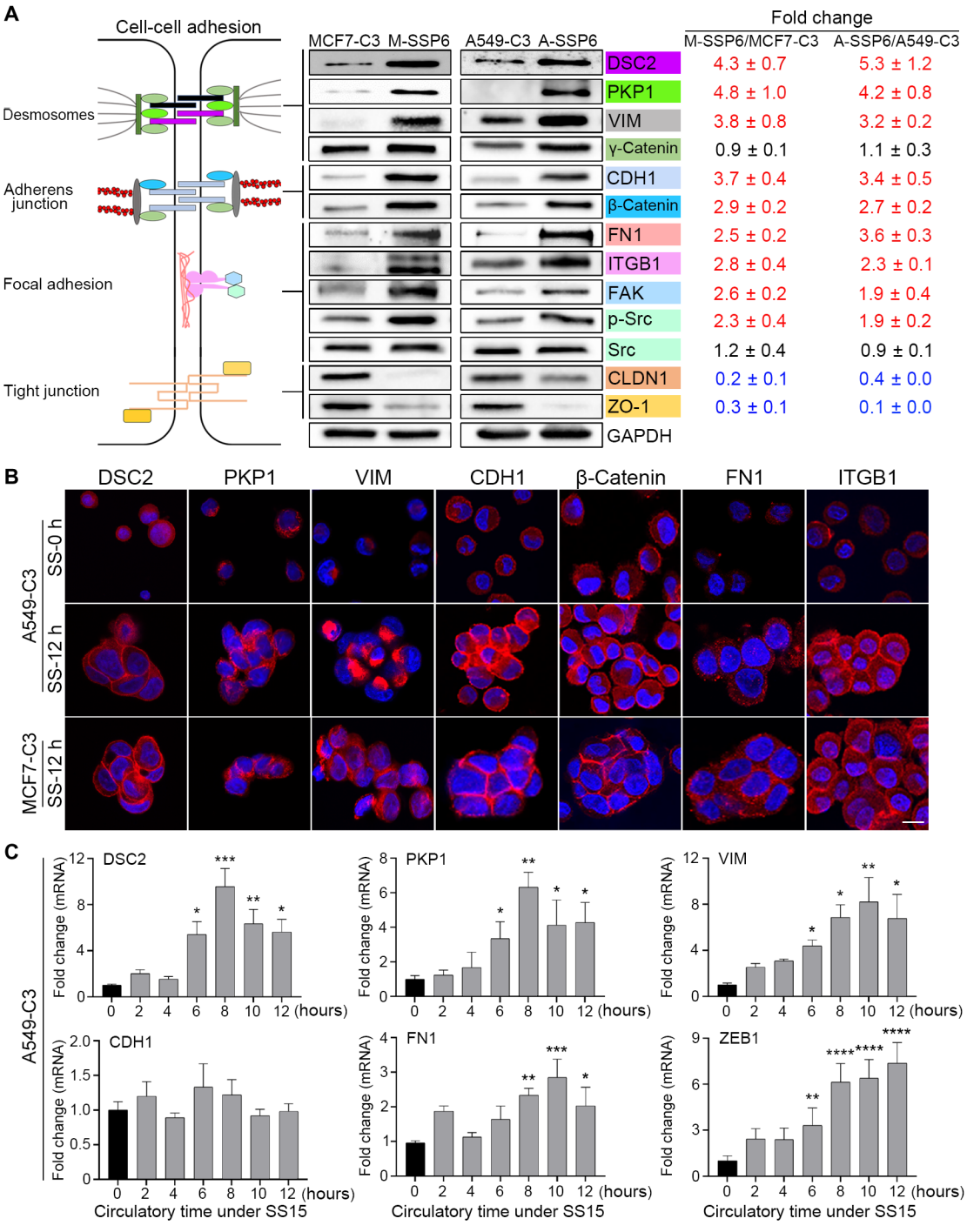

Fig. 4. Identification of adhesive molecules that were up-regulated in SSP6 cells. (**A**) Western blots showing the change in adhesive proteins in the M-SSP6 and A-SSP6 cells. Quantified data are presented as the means ± SD from three independent experiments. (**B**) Representative immunofluorescence (IF) staining images illustrating the distribution of DSC2, PKP1, vimentin (VIM), E-cadherin (CDH1), β-catenin, fibronectin (FN1), and integrin β_1 (ITGB1) in the A549-C3 and MCF7-C3 cells before and after SS15 treatment for 12 hours. Scale bar, 10 μm. (**C**) qRT-PCR results showing the normalized mRNA levels of DSC2, PKP1, VIM, CDH1, FN1, and ZEB1 in the A549-C3 cells under SS15 treatment at various time points. As glyceraldehyde-3-phosphate dehydrogenase (GAPDH) is a housekeeping gene whose mRNA level in A549-C3 cells at 0 hours was normalized to 1 and used as an internal reference for calculating the mRNA levels of the other tested genes. The results represent the means ± SD from three independent experiments. Significant differences were determined by one-way analysis of variance (ANOVA) (C). *$P < 0.05$, **$P < 0.01$, ***$P < 0.001$, and ****$P < 0.0001$.

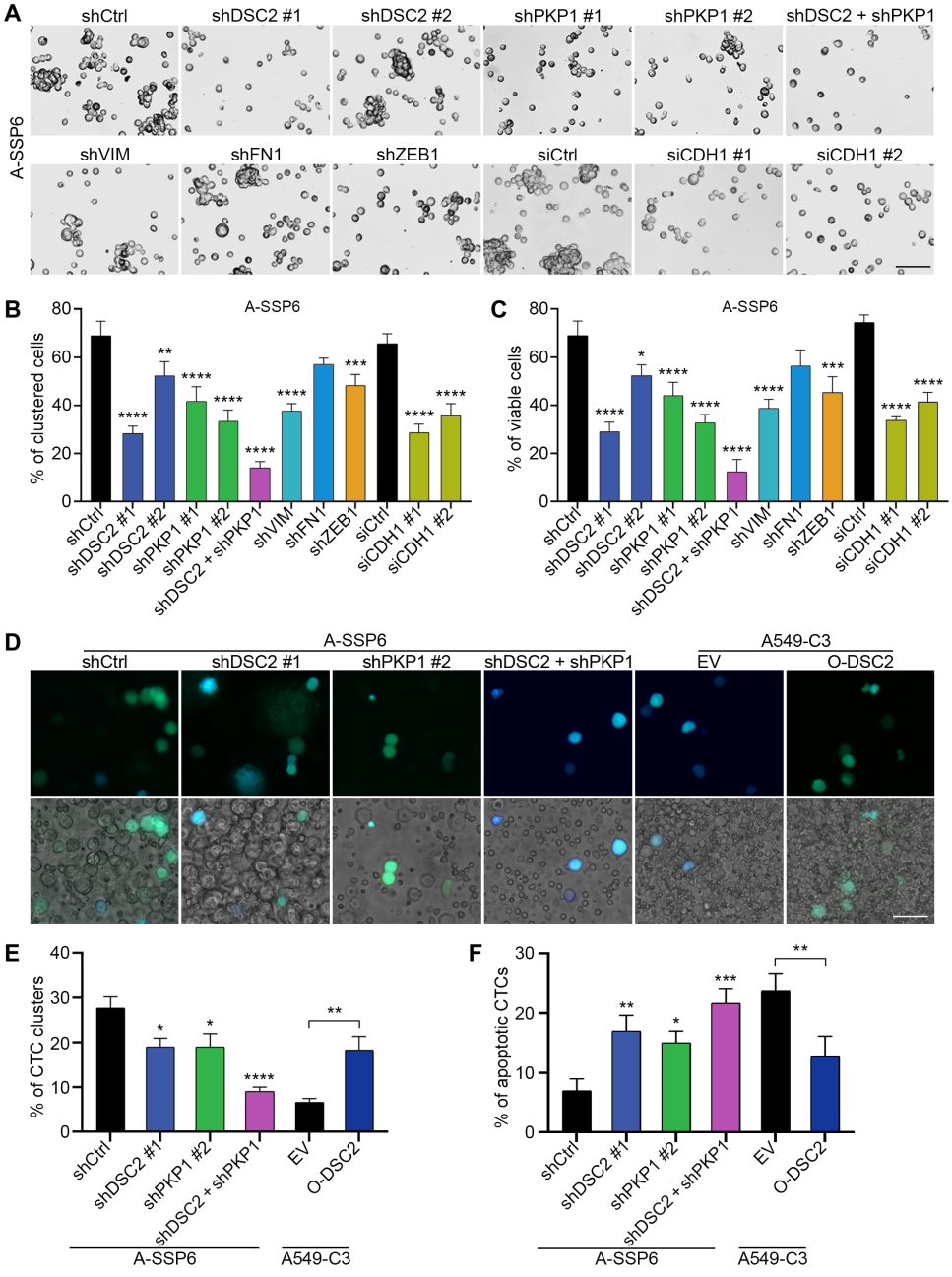

Fig. 5. The dual expression of DSC2 and PKP1 is important for cluster formation and survival in the circulation of A-SSP6 cells. (**A** to **C**) Representative phase images and quantified percentages of clustered and viable cells upon knockdown of the DSC2, PKP1, DSC2 + PKP1, VIM, FN1, ZEB1, and CDH1 genes in A-SSP6 cells circulated under SS15 for 10 hours (the results were quantified from three independent experiments, cell numbers of ≥300 for each independent experiment). shCtrl, negative control shRNA. Scale bar, 100 μm. (**D** to **F**) Representative images and quantified percentages of clustered and apoptotic cells obtained from mouse blood 4 hours after tail vein injection of the A-SSP6 cells upon knockdown of the expression of the DSC2, PKP1, and DSC2 + PKP1 or injection of A549-C3 cells upon overexpression of the DSC2 ($n = 5$ mice per group). EV, empty vector; O-DSC2, overexpression of DSC2. Scale bar, 50 μm. The results represent the means ± SD. Significant differences were determined by one-way ANOVA (B, C, E, and F) except for the differences between empty vector and overexpression of DSC2 in which Student's *t* test was used. $^{*}P < 0.05$, $^{**}P < 0.01$, $^{***}P < 0.001$, and $^{****}P < 0.0001$.

four possible combinations of shRNAs. The qRT-PCR and Western blot results showed that combination #3, which used shDSC2 #1 and shPKP1 #1, produced the best effects in reducing the mRNA levels of both DSC2 and PKP1 in the A-SSP6 cells (fig. S8A). When these two shRNAs were used to double knockdown of DSC2 and PKP1, they further reduced the ability of the A-SSP6 cells to form clusters and survive after circulatory treatment by more than 1.5- to 1.8-fold compared with that of the single knockdown of DSC2 and PKP1, respectively (Fig. 5, A to C).

We subsequently investigated whether DSC2 and PKP1 are important for cluster formation and cell survival in mouse circulation. A-SSP6 cells were transfected with gene-specific shRNAs alone or

in combination, and 2 million transfected cells were introduced into the bloodstream of NOD/SCID mice via tail vein injection. After 4 hours, blood samples were collected, and the red blood cells were lysed. The processed blood samples (100 μl) were visualized by live-cell FRET imaging microscopy and bright-field microscopy. Numerous FRET images were used to quantify the percentages of clustered CTCs and apoptotic CTCs. At least 200 CTCs were counted from five mice per group. The quantified results showed that single knockdown of DSC2 and PKP1 significantly reduced the percentage of clustered cells by 32 and increased the percentage of apoptotic cells by 147 and 126%, respectively, compared with those of the shRNA control group (Fig. 5, D to F). Double knockdown of DSC2 and PKP1 further decreased the ability of CTCs to form clusters by 52% and increased the apoptotic rates by 27 and 39% compared to the single knockdown of DSC2 and PKP1, respectively (Fig. 5, D to F).

To validate the important roles of DSC2 and PKP1 in cluster formation and cell survival, we overexpressed DSC2 in A549-C3 cells (fig. S8, C and D). The Western blot results showed that overexpression of DSC2 not only increased its own protein expression but also enhanced the protein expression of PKP1 (fig. S8D). The results of animal experiments showed that overexpression of DSC2 markedly increased the ability of CTCs to form clusters by 177% and decreased the apoptotic rates by 47%, compared to the A549-C3 cells transfected with an empty vector (Fig. 5, D to F). These results suggest that the presence of both desmosomal proteins of DSC2 and PKP1 is important for CTCs to form clusters and resist SS-induced cell death in circulation.

Knockdown of DSC2, DSC2/PKP1, VIM, FN1, and ZEB1 reduces the migration, invasion, cell adhesion, colony formation, and metastasis of A-SSP6 cells

As SSP6 cells displayed a higher capacity not only for cluster formation and survival in circulation (Fig. 2) but also for metastasis (Fig. 3), we then investigated which of the six candidate genes are involved in enhancing the metastatic capacity of these SSP6 cells. The results of Transwell migration and invasion assays revealed that knocking down the expression of DSC2, PKP1, DSC2 + PKP1, VIM, FN1, and ZEB1 effectively decreased the migration and invasion of the A-SSP6 cells (Fig. 6, A to C, and fig. S11) and that of the M-SSP6 cells (fig. S12) compared with those of the shRNA negative control groups.

Similarly, cell adhesion and colony-forming ability were also reduced after silencing DSC2, PKP1, DSC2 + PKP1, VIM, FN1, and ZEB1 in both the A-SSP6 (fig. S13) and M-SSP6 (fig. S14) cells. However, silencing CDH1 showed no effects on migration and invasion in the A-SSP6 cells (Fig. 6, A to C, and fig. S11A) or in the M-SSP6 cells (fig. S12). Silencing CDH1 significantly reduced cell adhesion and colony-forming ability of the A-SSP6 cells (fig. S13) but did not produce such an effect in the M-SSP6 cells (fig. S14).

On the basis of the in vitro results, we thus examined the effects of knocking down five of six candidate genes, DSC2, PKP1, VIM, FN1, and ZEB1, on lung colony formation using an experimental lung metastatic mouse model. Individual shRNAs or a combination of shDSC2 + shPKP1 was transfected into the A-SSP6 cells, and 1 million transfected cells were injected into the tail vein of NOD/SCID mice. Three weeks after injection, the numbers of GFP^+ foci were counted from each left side of the lung, and the quantified results showed that knocking down the expression of DSC2, DSC2 + PKP1, VIM, FN1, and ZEB1 significantly reduced the numbers of GFP^+ foci in the lung (Fig. 6, D and F). Among the six shRNA groups, shVIM and shZEB1 produced the best inhibitory effects on lung colony formation.

We then overexpressed VIM and ZEB1 in A549-C3 cells (fig. S8E) and observed that overexpressing either one of them markedly increased the number of lung foci (Fig. 6, E and F). Collectively, these in vitro and in vivo results indicated that among the five candidate genes, VIM and ZEB1 played more important roles than DSC2, PKP1, and FN1 in increasing SS-resistant A-SSP6 cells to home to the lung and grow into lung colonies in mice.

High expression levels of DSC2 and PKP1 correlate with tumor progression and a poor prognosis and are important for spontaneous metastasis

As DSC2 and PKP1 played important roles in cluster formation and survival, while VIM and ZEB1 played more important roles in other parts of the metastatic processes, we compared the levels of these four proteins between the lung tumors and adjacent tissues from patients with lung adenocarcinoma using immunohistochemistry (IHC) staining (Fig. 7A). The results in Fig. 7B show that there is a positive correlation between the IHC score of DSC2 and the IHC score of PKP1. This positive correlation suggests that these two proteins might be coexpressed in lung tumors (Fig. 7B). Moreover, the level of DSC2 staining was significantly higher in lung tumors than in the adjacent tissues, and the level of PKP1 was also notably higher in lung tumors than in the adjacent tissues (Fig. 7, A, C, and D). In contrast, as both lung tumors and adjacent tissues showed strong staining with VIM and ZEB1, no significant difference was found between the tumor and adjacent tissues (Fig. 7, A, E, and F).

We also performed the same IHC staining on samples of patients with breast cancer and obtained several findings. First, the staining intensities of PKP1 in both the primary and metastatic breast tumors were much stronger than that of DSC2, indicating that PKP1 was expressed at higher levels in breast tumors (Fig. 7, G to I). Second, for both DSC2 and PKP1, their IHC score values in the primary and metastatic tumors were significantly higher than that in the normal tissues (Fig. 7, H and I). Third, the staining of PKP1 in the metastatic tumors was much stronger than that in the primary tumors (Fig. 7I). Fourth, although the staining intensity of VIM was quite high, no significant difference was observed among normal tissues, primary tumors, and metastatic tumors (Fig. 7, J and K). Fifth, a very weak staining signal of ZEB1 was observed in all three types of breast samples (Fig. 7, J and L).

Kaplan-Meier plots revealed that high expressions of DSC2 and PKP1 were correlated with shorter overall survival (OS) in patients with lung and breast cancer (Fig. 8, A and B). Moreover, high levels of DSC2 and PKP1 were found to correlate with lower distant metastasis-free survival (DMFS) in patients with breast cancer (Fig. 8C). In contrast, the high levels of VIM and ZEB1 were correlated with longer OS in patients with lung cancer (Fig. 8A) and had no significant correlations with the OS and DMFS of patients with breast cancer (Fig. 8, B and C). Therefore, both IHC staining and meta-analyses indicated that DSC2 and PKP1 are expressed at higher levels in lung and breast tumors and that these high expression levels are correlated with the poor prognosis of cancer development.

On the basis of the clinical results, we then determined the importance of DSC2 and PKP1 for spontaneous metastasis using a lung orthotopic model. Three million SS-resistant A-SSP6 cells with shCtrl or shDSC2 + shPKP1 were implanted in the right lungs of NOD/SCID

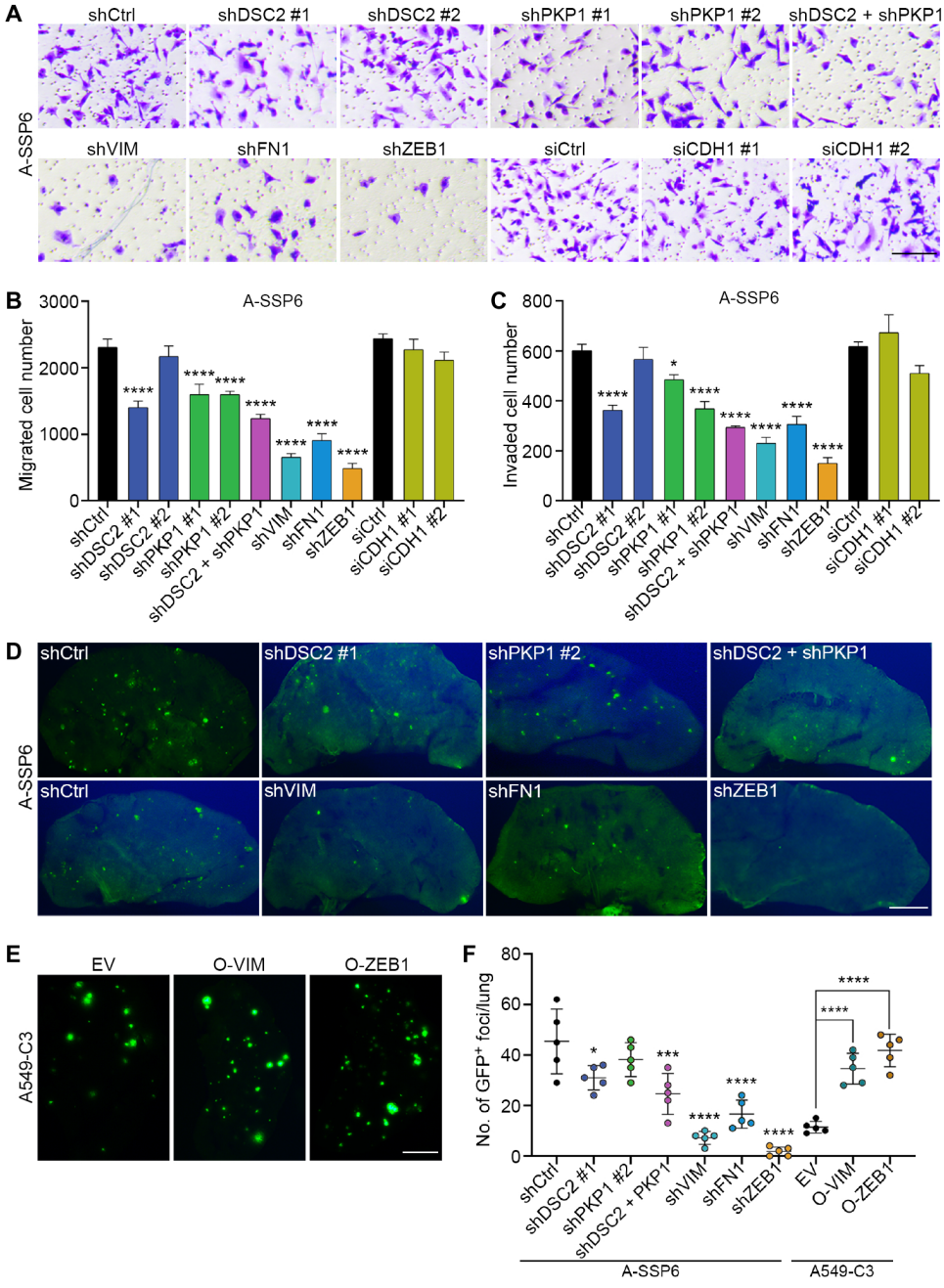

Fig. 6. Knockdown of DSC2, DSC2 + PKP1, VIM, FN1, or ZEB1 effectively reduced the metastatic potential of A-SSP6 cells. (**A** and **B**) Representative images and quantified results of the migrated cells with 20,000 cells seeded per insert for 24 hours after silencing DSC2, PKP1, DSC2 + PKP1, VIM, CDH1, FN1, and ZEB1 in the A-SSP6 cells. Two Transwell inserts were used in each migration assay, which was repeated two more times. Scale bar, 200 μm. (**C**) Quantified numbers of invading cells with 20,000 cells seeded on the Matrigel-coated membrane of the Transwell insert for 24 hours after silencing DSC2, PKP1, DSC2 + PKP1, VIM, CDH1, FN1, or ZEB1 in A-SSP6 cells. Two Transwell inserts were used in each invasion assay, which was conducted in triplicate. (**D** to **F**) Representative images and quantified results of the lung colony-forming ability upon DSC2, PKP1, DSC2 + PKP1, VIM, FN1, or ZEB1 knockdown in A-SSP6 cells for 21 days or overexpression of VIM or ZEB1 in A549-C3 cells for 30 days ($n = 5$ mice per group). O-VIM, overexpression of VIM; O-ZEB1, overexpression of ZEB1. Scale bars, 1 mm (D and E). The data are shown as the means ± SD. Significant differences were determined by one-way ANOVA (B, C, and F). *$P < 0.05$, ***$P < 0.001$, and ****$P < 0.0001$.

mice. Four weeks after implantation, the mice were euthanized, and all organs were removed and examined by fluorescence and phase microscopy. There were no differences in the primary tumor growth or body weight of the mice between the shCtrl and shDSC2 + shPKP1 groups (Fig. 8, D to F). For metastatic tumors, we observed that four of five mice from the shCtrl group had large metastatic tumors located in the liver, intestine, or brain. Only two of seven mice from the shDSC2 + shPKP1 group had small metastatic tumors in the liver, and no metastatic tumors were found in any other organs (Fig. 8, D and G).

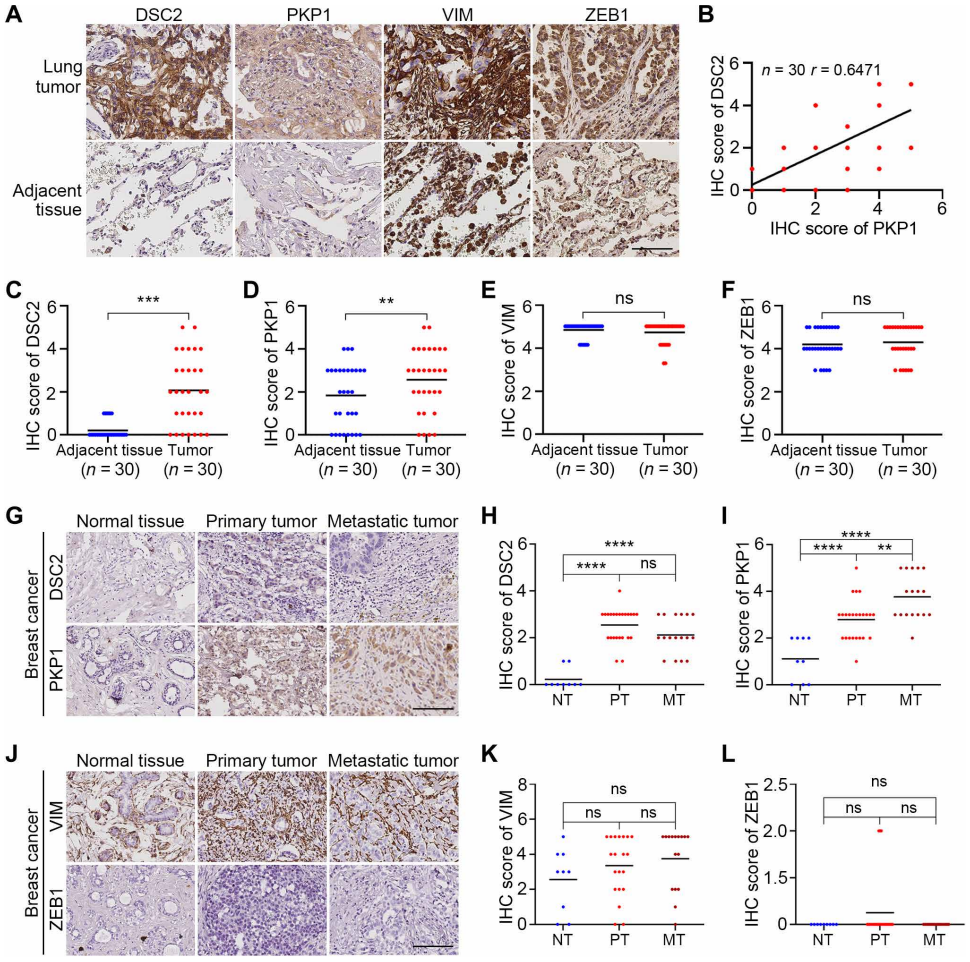

Fig. 7. Clinical significance of DSC2 and PKP1 in lung and breast cancer. (**A**) Representative images of IHC staining for DSC2, PKP1, VIM, and ZEB1 between lung tumors and adjacent tissues from patients with lung cancer. Scale bar, 100 μm. (**B**) The positive correlation between the IHC score of DSC2 and that of PKP1 in patients with lung cancer ($n = 30$). (**C** to **F**) Plots showing the IHC scores of DSC2, PKP1, VIM, and ZEB1 between the adjacent tissues and human lung tumors ($n = 30$). Each dot represents one patient. (**G** to **L**) Representative images and quantified IHC scores of DSC2, PKP1, VIM, and ZEB1 among normal tissues, primary tumors, and metastatic tumors in patients with breast cancer. Plots showing the IHC scores for DSC2, PKP1, VIM, and ZEB1 in normal tissues (NT), primary tumors (PT), and metastatic tumors (MT). Scale bars, 100 μm. Significant differences were determined by Student's *t* test (C to F) and one-way ANOVA (H, I, K, and L). $^{**}P < 0.01$, $^{***}P < 0.001$, and $^{****}P < 0.0001$.

Elucidation of the underlying mechanisms through which DSC2 and PKP1 support the survival and metastasis of SS-resistant cancer cells

To investigate how A-SSP6 cells can survive circulatory treatment, we first determined the levels of prosurvival proteins in A-SSP6 cells. The results showed that the levels of three proteins or their phosphorylated forms were significantly up-regulated: phosphorylated AKT (p-AKT; 4.9-fold), B-cell lymphoma 2 (Bcl-2) (7.3-fold), and phosphorylated extracellular signal–regulated kinase 1 and 2 (p-ERK1/2; 2.5-fold) in the A-SSP6 cells compared with the A549-C3 cells (Fig. 9A).

We then reduced the expression of DSC2, PKP1, and DSC2 + PKP1 with shRNAs and observed three findings. First, we found that knockdown of the expression of DSC2, PKP1, and DSC2 + PKP1 significantly reduced the levels of the prosurvival proteins of p-AKT and Bcl-2 but had no obvious effect on p-ERK1/2 (Fig. 9B). Second, reducing the expression of DSC2 also reduced the level of PKP1 by 50%, while reducing the level of PKP1 did not strongly decrease the level of DSC2. Third, double knockdown of DSC2 and PKP1 reduced the level of VIM by 60%, while single knockdown of DSC2 or PKP1 did not significantly reduce the VIM levels. Furthermore, we found that knockdown of VIM reduced the level of DSC2 by 40% and decreased the level of PKP1 by 50% (Fig. 9B). These results suggest that the collaborative interactions among DSC2, PKP1, and VIM may be important to maintain the high presence of individual desmosomal proteins in SS-resistant cells.

Next, we examined the effect of gene silencing on other adhesive proteins. We found that knockdown of DSC2, PKP1, and DSC2 + PKP1 reduced the protein level of CDH1 by 30 to 40%, while silencing VIM did not affect the protein level of CDH1, indicating that DSC2 and PKP1 may positively regulate CDH1 in the A-SSP6 cells (Fig. 9, B and H).

Furthermore, double knockdown of DSC2 + PKP1 and knockdown of VIM significantly decreased the level of ITGB1 by 40 to 50%, but single knockdown of DSC2 or PKP1 only slightly reduced the level of ITGB1 (Fig. 9B). As single knockdown of DSC2 or PKP1 produced a weaker effect than double knockdown of DSC2 and PKP1 in reducing the VIM protein (Fig. 9B), we wanted to examine whether VIM can link DSC2/PKP1 with ITGB1. To do this, we first

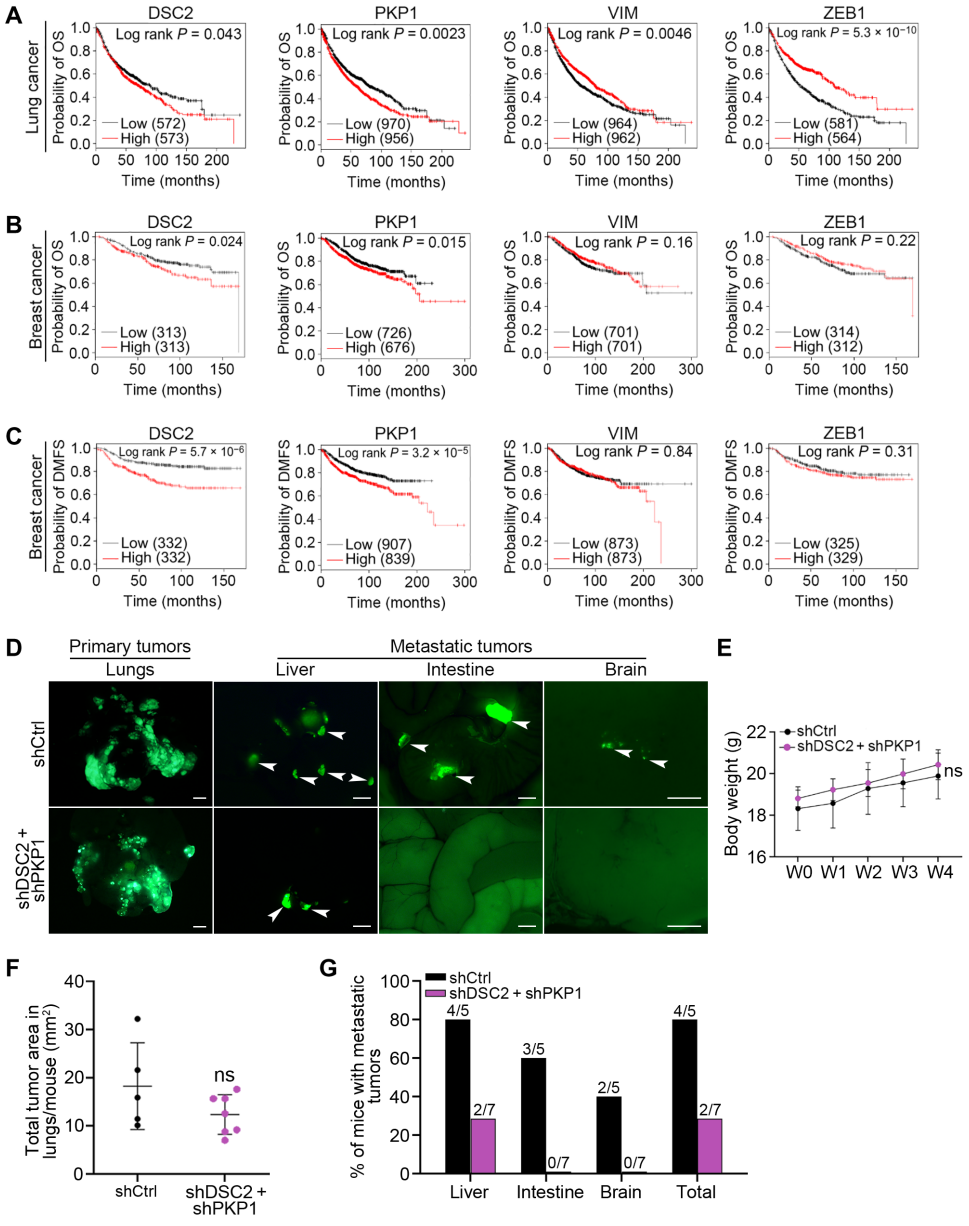

Fig. 8. Clinical relevance of DSC2 and PKP1 in lung and breast cancer and their importance in spontaneous metastasis. (**A** to **C**) Kaplan-Meier plots of OS and DMFS curves in patients with lung and breast cancer. (**D**) Three million A-SSP6 cells after DSC2 + PKP1 knockdown were implanted into the right lung, and representative images of the lung, liver, intestine, and brain in the shCtrl or shDSC2 + shPKP1 groups using the lung orthotopic metastatic mouse model are shown. Scale bars, 1 mm (primary lung tumor) and 200 μm (liver, intestine, and brain). White arrowheads indicate metastatic tumors ($n = 5$ to 7 mice per group). (**E**) Body weights of mice injected with shCtrl and shDSC2 + shPKP1 groups after orthotopically implantation for 1 to 4 weeks ($n = 5$ to 7 mice per group). (**F**) Quantified total tumor area in five pieces of lungs is shown 4 weeks after implantation ($n = 5$ to 7 mice per group). (**G**) Quantified percentage of mice with liver, intestine, brain, and total metastasis ($n = 5$ to 7 mice per group). Significant differences were determined by Student's *t* test (F) or two-way ANOVA (E).

overexpressed DSC2 in A549-C3 cells and found that its overexpression elevated the protein levels of DSC2 and PKP1 (fig. S8D), as well as the levels of VIM and ITGB1 (Fig. 9D). Moreover, when VIM was knocked down in A549-C3 cells that overexpressed DSC2, the expression of ITGB1 was significantly decreased (Fig. 9E). We thus propose that the DSC2 and PKP1 might function on ITGB1 via VIM (Fig. 9H).

As ITGB1 usually binds to extracellular matrix components such as FN1, we evaluated the importance of their presence to each other and found that knockout of ITGB1 significantly decreased the level of FN1, but knockdown of FN1 had a minor impact on ITGB1, which suggests that FN1 may use ITGB1 to transmit its signals (Fig. 9, C and F). We further examined the possible downstream signaling molecules of ITGB1 and FN1 and found that knockout of ITGB1 or knockdown of FN1 significantly reduced the levels of FAK, p-Src, p-AKT, and p-ERK1/2 (Fig. 9, C and F). In addition, knockdown of VIM not only reduced DSC2, PKP1, ITGB1, p-AKT, and p-ERK1/2 (Fig. 9B) but also decreased the levels of FAK and p-Src in A-SSP6 cells (Fig. 9G).

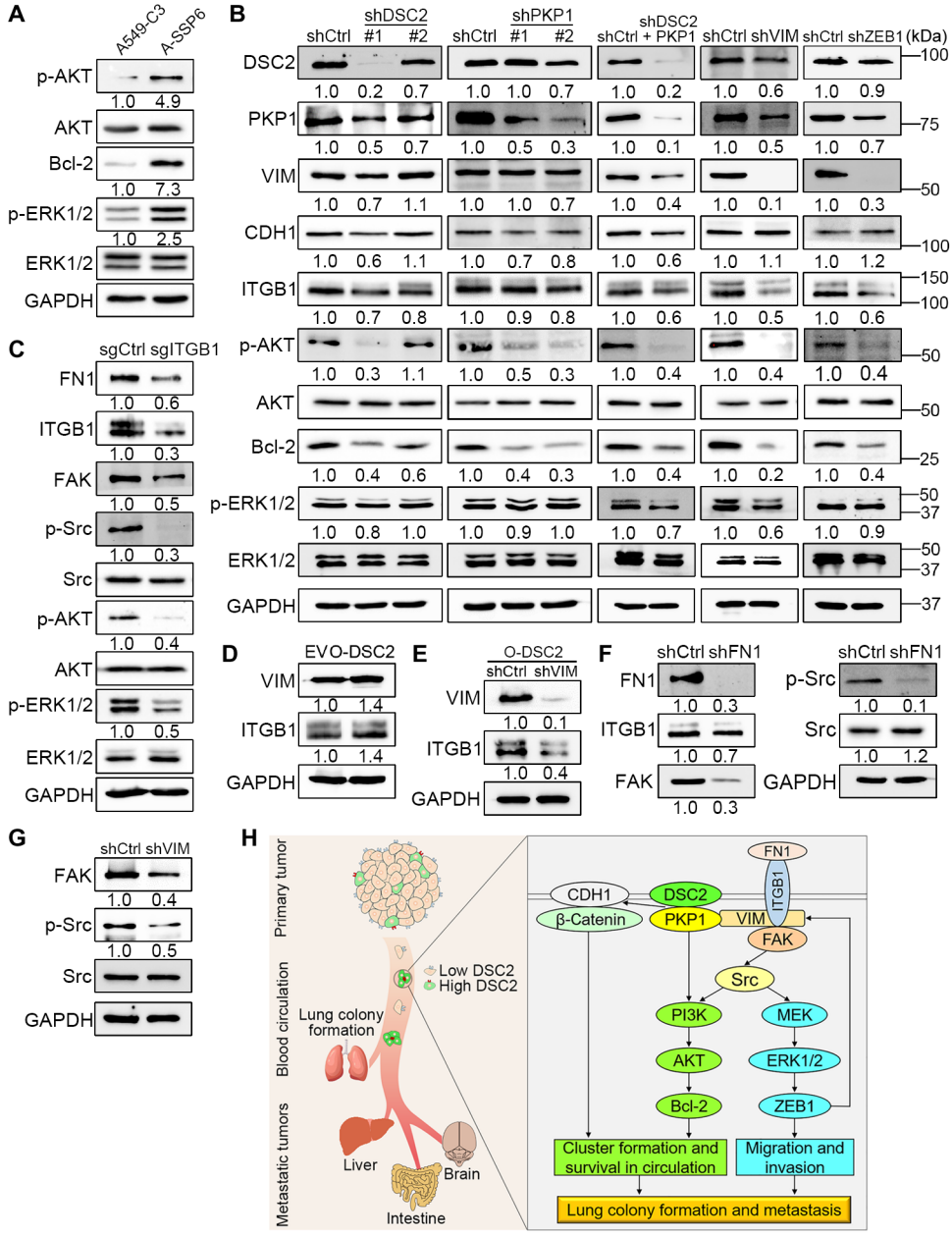

Fig. 9. Signaling pathways of DSC2 and PKP1. (**A**) Western blots showing the higher expression of p-AKT, Bcl-2, and p-ERK1/2 in A-SSP6 cells. (**B**) Western blots showing the knockdown effects of DSC2, PKP1, DSC2 + PKP1, VIM, and ZEB1 on themselves and other proteins in A-SSP6 cells. (**C**) Western blots showing the effects of knockout ITGB1 on various indicated proteins in A-SSP6 cells. (**D**) DSC2 was overexpressed in A549-C3 cells and Western blots showing the up-regulation of VIM and ITGB1. (**E**) DSC2 was first overexpressed in A549-C3 cells, and then VIM was knocked down in these overexpressed cells, Western blots showing the down-regulation of VIM and ITGB1 after knockdown of VIM. (**F**) Western blot results indicating that shFN1 reduced the levels of ITGB1, FAK, and p-Src. (**G**) Western blotting showing that the levels of FAK and p-Src were decreased after VIM was knocked down. (**H**) The left side of the schematic illustration shows that CTCs with high levels of DSC2 can form clusters, survive in circulation, and subsequently form lung colonies by tail vein injection or metastasize to the liver, intestine, and brain in the lung orthotopic model. The right side of the schematics illustrates the proposed signaling pathways through which DSC2/PKP1 and VIM support cluster formation, cell survival in circulation, lung colony formation, and metastasis.

Moreover, inhibiting FAK with its inhibitor 14 reduced the total level of FAK and significantly reduced p-Src, p-AKT, and p-ERK1/2 but not the total levels of these three proteins. Furthermore, inhibiting Src with dasatinib produced similar reductive effects on p-Src, p-AKT, and p-ERK1/2 without affecting the total protein level of FAK (Fig. 10A). In addition, inhibiting PI3K with dactolisib substantially decreased the levels of p-AKT and Bcl-2 (Fig. 10B). All the results presented in this section indicate that DSC2/PKP1/VIM can work through FN1/ITGB1 to transmit its signals to the FAK-Src axis to activate both the PI3K/AKT/Bcl-2 and mitogen-activated protein kinase kinase (MEK)/ERK1/2 signaling pathways in SS-resistant A-SSP6 cells (Fig. 9H).

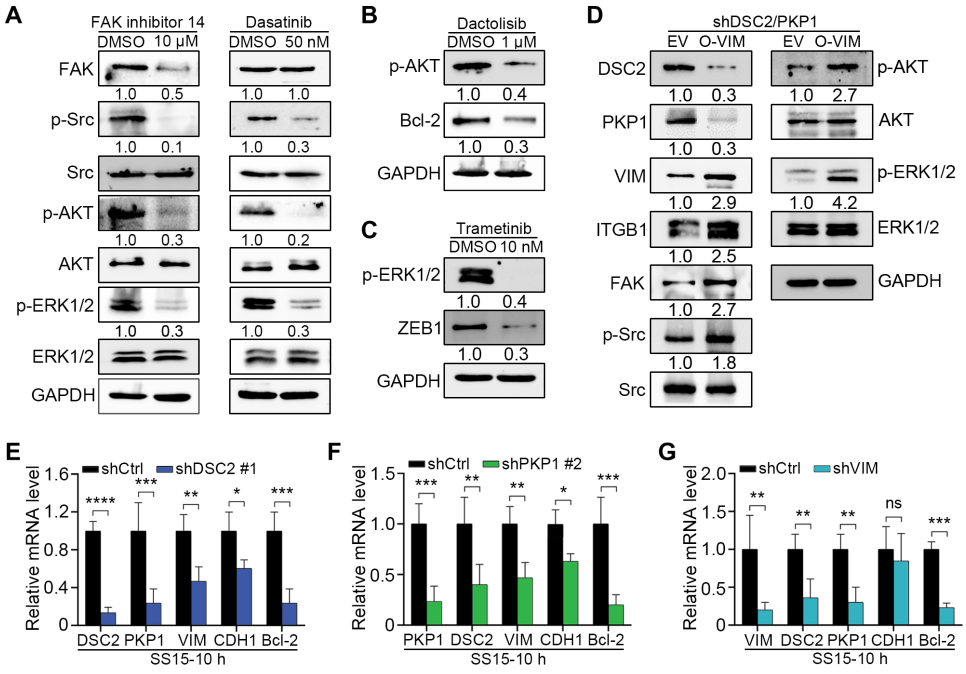

Fig. 10. Studying the interactions between DSC2, PKP1, and VIM and their downstream molecules. (**A**) Western blot results revealing that treating A-SSP6 cells with the FAK inhibitor 14 (10 μM) or the Src inhibitor (50 nM) for 24 hours reduced the levels of FAK, p-Src, p-AKT, and p-ERK1/2. DMSO, dimethyl sulfoxide. (**B** and **C**) Western blotting of p-AKT, Bcl-2, p-ERK1/2, and ZEB1 in the A-SSP6 cells treated with the PI3K inhibitor dactolisib (1 μM) or MEK inhibitor trametinib (10 nM) for 24 hours. (**D**) Western blots showing the increases in VIM, ITGB1, FAK, p-Src, p-AKT, and p-ERK1/2 after overexpression of VIM in A-SSP6 cells with double knockdown of DSC2 and PKP1. (**E** to **G**) qRT-PCR results showing the knockdown effects of shDSC2 (E), shPKP1 (F), and shVIM (G) on the mRNA levels of DSC2, PKP1, VIM, and Bcl-2. As GAPDH is a house-keeping gene, it was used as an internal control for qRT-PCR experiments. The mRNA level in shCtrl group of A-SSP6 was normalized to 1. The results are the means ± SD from three independent experiments. Significant differences were determined by two-way ANOVA (E to G). *$P < 0.05$, **$P < 0.01$, ***$P < 0.001$, and ****$P < 0.0001$.

We also examined the impact of knocking down ZEB1 expression and found that it significantly reduced the protein levels of VIM, ITGB1, p-AKT, and Bcl-2 but did not affect the levels of ERK1/2 and p-ERK1/2, indicating that ZEB1 may up-regulate the expression of VIM (Fig. 9B). We then used the MEK inhibitor trametinib to inhibit the phosphorylation of ERK1/2, which also substantially reduced the level of ZEB1 protein (Fig. 10C). Last, we knocked down the high expression of DSC2 and PKP1 with shDSC2/PKP1 and overexpressed VIM in A-SSP6 cells. The results showed that these treatments greatly elevated the levels of ITGB1, FAK, p-Src, p-AKT, and p-ERK1/2 (Fig. 10D). Taken from the previous findings that shDSC2/PKP1 reduced the levels of VIM, ITGB1, p-AKT, and p-ERK1/2 (Fig. 9B), we propose that DSC2/PKP1 may use VIM to stimulate ITGB1/FAK/Src, which activates MEK/ERK1/2 and ZEB1. ZEB1, in turn, increased the expression of VIM, which is important to stabilize the desmosome structure consisting of DSC2, PKP1, and VIM (Fig. 9H).

Last, we examined the effects of knocking down the expression of DSC2, PKP1, and VIM on their mRNA levels during circulatory treatment. A-SSP6 cells were circulated under SS15 for 12 hours, and their mRNA levels were measured by qRT-PCR. The results showed that shRNAs against DSC2, PKP1, and VIM not only strongly reduced their own mRNA levels but also significantly reduced the mRNA levels of other desmosomal members. These three sets of shRNAs also significantly reduced the mRNA levels of Bcl-2 by 80%, while shRNAs of DSC2 and PKP1 slightly reduced the mRNA levels of CDH1, and shRNA of VIM did not affect the expression of CDH1 (Fig. 10, E to G). These results provide more insights into why cancer cells with high expression of DSC2, PKP1, and VIM are prone to form clusters in circulation and why those clustered cells are more resistant to SS-induced cell death (Fig. 9H).

DISCUSSION

CTC clusters have been shown to have a higher survival and metastatic capacity than single CTCs (*31*–*33*), and the presence of these CTC clusters was correlated with a poor prognosis of cancer development (*33*). In this study, we found that the high expression of two desmosomal proteins, DSC2 and PKP1, is important for cancer cells to form clusters, to survive in the bloodstream, and to colonize the lung and metastasize to other organs in mice.

The desmosome is an important structure for cell-cell adhesion. Desmosomes play important roles in various biological processes, including cell growth, invasiveness, adhesion, and apoptosis (*36*–*38*). Previous studies have reported that high expression of DSC2 increased cell aggregation (*39*–*41*), and high levels of PKP1 and DSG3 were found in disseminated tumor cell clusters (*42*). In our study, we found that both DSC2 and PKP1 were expressed at high levels, while the mRNA level of DSG3 was not detectable in SS-resistant cells. High expression of PG has been found in CTC clusters of patients with breast cancer (*33*); however, high levels of PG were detected in both SS-resistant and parental cells in our study.

When cells are exposed to mechanical stress, desmosomes and intermediate filaments provide the mechanical stability required to maintain cell-cell adhesion and integrity (*38*). Although the

intermediate filament keratin (K14) was highly expressed in the clustered breast cancer cells and depletion of K14 decreased distant metastasis (*42*), no significant up-regulation of K14 mRNA was found in our RNA-seq analysis. Rather, a significant elevation in VIM was detected in SS-resistant cells, and knockdown of VIM significantly reduced their ability to form lung colonies.

In addition to desmosomal proteins, the levels of adherens junction proteins (CDH1 and β-catenin) and focal adhesion proteins (FN1, ITGB1, and FAK) were also up-regulated in SS-resistant cells. Previous studies have reported that several adhesion-related genes were enriched in clustered cells and conferred metastatic potential (*31*, *34*, *42*–*47*). Moreover, snail directed collective migration in squamous carcinoma cells by inducing the expression of a tight junctional protein, CLDN11 (*47*). In addition, some other junction-related proteins, such as ZO-1 and CDH1, have been revealed to play important roles in collective migration (*43*, *44*). In our study, the levels of two tight junction proteins (CLDN1 and ZO-1) were greatly reduced, and the level of snail was not significantly changed according to RNA-seq analyses in SS-resistant cells. Although the levels of CDH1 were elevated in SS-resistant cells, knockdown of CDH1 only affected cluster formation and survival but not cell migration and invasion. In addition, high levels of the stemness marker CD44 were found in CTC clusters, which mediated cluster formation and promoted tumor cell survival and metastasis (*34*). However, no significant change in CD44 mRNA levels was detected in SS-resistant cells in our study.

Previously, several studies reported that the PI3K/AKT pathway and Bcl-2 were activated in fluid SS-exposed cancer cells to promote motility, proliferation, or survival (*18*, *48*–*50*). Moreover, CTCs isolated from the bloodstream that had higher levels of PI3K, AKT, or Bcl-2 displayed higher levels of cell survival (*23*, *51*). In this study, we connected the roles of DSC2 and PKP1 in facilitating cancer cells to form clusters in circulation to activating the PI3K/AKT/Bcl-2–mediated pathway to increase cell survival.

DSC2 and PKP1 have been reported to be both oncogenes and tumor suppressors in previous studies (*23*, *52*–*56*). In this study, we found that high levels of DSC2 and PKP1 were also important for maintaining the high expression of VIM, which subsequently stimulated FN1/ITGB1/FAK/Src/MEK/ERK/ZEB1-mediated metastasis. Compared to the previously reported function of VIM and ZEB1 in clustered cells (*57*, *58*), our findings provide new insights into their roles during metastasis.

As VIM and ZEB1 are important regulators of EMT, we propose that SS-resistant cells can also stimulate the EMT process to increase cluster formation and cell survival. The mechanisms of how EMT functions in CTCs have been reported previously. For example, the EMT-tissue factor regulatory axis can activate coagulation pathways and form a fibrin/platelet-rich microclot around CTCs to physically protect CTCs from SS, immune attack, and anoikis (*59*). Another EMT-driven survival mechanism of CTCs in the bloodstream involves the formation of microtubule protrusions (termed microtentacles), which are supported by VIM filaments and are up-regulated by snail and twist (*58*, *59*). However, the level of twist was very low in SS-resistant cells.

In this study, we found that the high expressions of adhesion molecules of DSC2, PKP1, and EMT markers of VIM and ZEB1 were important for SS-resistant cells to survive in circulation and gain metastatic abilities. Our observations are partially consistent with previous findings that CTCs expressed both epithelial and mesenchymal markers (*60*, *61*), and coexpression of these markers enhanced invasiveness, metastasis, and poor survival of breast cancer cell in comparison to the expression of VIM alone (*62*). In comparison to the previous studies that identified cytokeratins as the epithelial markers (*61*, *62*), our study indicated DSC2 and PKP1 as the new epithelial markers, which can also form hybrid EMT with the mesenchymal marker of VIM. As the desmosomal proteins of DSC2 and PKP1 can serve as anchors to dock more VIM molecules, a hybrid EMT consisting of DSC2, PKP1, and VIM can help CTCs to form clusters to resist the destructive effects of shear force in circulation. Moreover, this hybrid EMT can also activate the downstream signaling molecules of VIM including ITGB1, FAK, Src, MEK, ERK1/2, and ZEB1 to promote metastasis. Hence, our findings support the recently emerging hypothesis that a hybrid EMT status may be responsible for metastasis.

Because of the low number of CTC clusters in blood samples, it is challenging to use clinically isolated CTC clusters to elucidate the signaling pathways of cluster formation. To overcome this limitation, people have developed various systems to generate clustered cancer cells under suspension conditions (*42*, *58*, *63*), such as by shaking cells in a flask (*64*) or using a shorter time of trypsinization to produce cell clumps (*33*). Many studies also used various methods to generate fluid conditions, including stirring bath (*65*), cone and plate (*14*, *66*), syringe with needle (*10*, *26*, *28*, *49*), parallel plate (*48*, *67*) microfluidic devices (*68*), and circulatory system (*69*). In this study, we used a microfluidic circulatory system that allows the injected cells to continuously circulate under a pulsatile shear force similar to that of a human artery under a resting state with a heartbeat of 70 beats/min (*15*, *17*). The advantage of this system is that we can control the levels of SS; however, it cannot fully represent the actual conditions that CTCs confront in the human bloodstream.

Another limitation of our current system is that it does not include immune cells such as neutrophils, monocytes, macrophages, NK cells, and T cells, which also interact with CTCs or CTC clusters to affect metastatic progression (*70*, *71*). For example, the neutrophil can directly interact with CTCs that form CTC-neutrophil clusters to increase the metastatic potential of cancer cells. CTC clusters are less sensitive to NK-mediated suppression than single CTCs (*71*). In addition, tumor killing neutrophils have been found to kill cancer cells through the production of hydrogen peroxide (*72*). In the future, we will validate the findings obtained from our circulatory system with CTCs isolated from patients with cancer. Furthermore, we will investigate the effects of SS on cell-cell interactions between CTCs and other blood cells or platelets.

In summary, our results suggest that SS can elevate the levels of DSC2, PKP1, VIM, ZEB1, and FN1 in circulated lung and breast cancer cells. The elevated expression of DSC2 and PKP1 can activate PI3K/AKT or CDH1 to increase cluster formation to resist SS-induced cell death. DSC2/PKP1 can also function via VIM-ITGB1 to activate the PI3K/AKT and MEK-ERK1/2 pathways to increase cell survival and lung metastatic tumor formation. Last, higher expression of DSC2 and PKP1 were correlated with lower OS and worse disease progression in patients with breast and lung cancer. These findings suggest that CTCs might use the desmosomal proteins DSC2 and PKP1 to mediate cluster formation. If these findings can be validated in clinical CTCs, then these two proteins can potentially be used as new diagnostic markers and therapeutic targets for metastatic CTCs.

MATERIALS AND METHODS

Cell lines and cell culture

The breast cancer cell lines MCF7, T47D, and BT474; the lung cancer cell line A549; the colorectal cancer cell line HCT-116; human umbilical vein endothelial cells (HUVECs); and the human embryonic kidney cell line 293T were obtained from the American Type Culture Collection and cultured in Dulbecco's modified Eagle's medium (DMEM; #12100046, Thermo Fisher Scientific, USA) supplemented with 1% penicillin-streptomycin antibiotics (#15140122, Thermo Fisher Scientific, USA) and 10% FBS (#10270-106, Gibco, USA). MCF7-C3 and A549-C3 cells were generated by transfecting a sensor C3 plasmid that encodes a FRET-based biosensor. These two cell lines can stably express sensor proteins that can emit green fluorescence if the sensor cells are alive and emit blue fluorescence when caspase-3/7 is activated when cells undergo apoptosis (*15*, *73*).

Generation of SS in a microfluidic circulatory system and FRET-based apoptotic assay

A microfluidic circulatory system was developed in our previous study, which includes a cell-holding reservoir covered with a cotton filter to prevent airborne contamination and evaporation of culture medium, a connecting tube, a peristaltic pump (Ismatec), and a 1.5-m-long circulatory tube with a diameter of 500 μm (Ismatec). This system can generate various levels of pulsatile SS that are present in the bloodstream of the human vascular system. The SS can be calculated on the basis of Poiseuille's equation, $\tau = 4Q\eta/\pi R^3$, where τ is the SS measured in dynes per square centimeter, Q is the flow rate in cubic centimeters per second, η is the dynamic viscosity of the fluid (0.01 dyne·s/cm^2), and R is the radius of the tubing (250 μm) (*15*, *17*, *74*). In this study, we chose SS15 as it is the average SS present in the human artery (*10*). To prevent cell attachment to the tubing, the whole system was precoated with 1% Pluronic F-127 (#P2443, Sigma-Aldrich, USA) for 1 hour.

Cancer cells were trypsinized and resuspended in fresh culture medium at a density of 2×10^5 cells/ml. One milliliter of cell suspension was added to the microfluidic system and circulated under SS15 for various time points. For live-cell imaging, the pump was switched off to stop the medium flow, and the circulated cells were collected and added to a confocal dish for FRET imaging and to a 96-well plate for the MTT assay.

MTT assays

Cells were collected after circulatory treatment, and 100 μl of circulated cancer cells was seeded in 96-well plates. Then, 10 μl of sterilized MTT (#M2128, Sigma-Aldrich, Germany) solution was added at a final concentration of 0.5 mg/ml. After 4 hours, another 100 μl of 10% SDS solution containing 0.01 M HCl was added to dissolve the crystallized MTT product formazan for over 12 hours. The absorbance of the MTT reaction was measured at 595 nm by a plate reader (PerkinElmer VICTOR X3).

Cell proliferation assay

A suspension of 3000 cells in 100 μl of culture medium was seeded into each well of a 96-well plate and incubated at 37°C for 0, 24, 48, 72, and 96 hours. The cell growth rate was determined by MTT assays at each indicated time point.

Anoikis resistance analysis using FRET imaging

SSP6 or parental cells were seeded into a six-well ultralow attachment plate (#3471, Corning, USA) at a density of 2×10^5 cells per 2 ml in normal culture medium in each well. After 36 or 72 hours of incubation in a CO_2 incubator at 37°C, cancer cells were imaged for FRET imaging analysis by a Carl Zeiss microscope (Axio Observer Germany).

Tumor sphere formation assay

Two hundred cancer cells were seeded into each well of a 96-well ultralow attachment U-bottom plate (#7007, Corning, USA), and tumor spheres were imaged weekly by a Carl Zeiss microscope. The images were analyzed by the fluorescence intensity.

Transwell migration and invasion assays

Cells were tested for their migratory and invasive ability to cross a membrane with a pore size of 8 μm in the Transwell chamber (#3422, Corning, USA). For the migration assay, the cells were trypsinized and resuspended in DMEM without serum. A suspension containing 2×10^4 cells in 100 μl was placed in the upper chamber, while 600 μl of DMEM with 10% FBS was added to the lower chamber. After 24 hours for A549-C3 and A-SSP6 or 48 hours for MCF7-C3 and M-SSP6 of incubation in a CO_2 incubator at 37°C, the cells on the top side of the Transwell membrane were removed by a cotton swab, whereas the cells on the bottom side were fixed with 4% paraformaldehyde (PFA; #158127, Sigma-Aldrich, Germany) for 15 min and stained with 0.5% crystal violet (#C6158, Sigma-Aldrich, Germany) for 15 min. Then, the membrane was cut off from the Transwell chamber and mounted onto a glass slide with mounting medium (#06522, Sigma-Aldrich, Germany).

For the invasion assay, all the procedures were the same as those described in the migration assay except that the upper chamber was precoated with 100 μl of Matrigel (#356230, Corning, USA) at 37°C for 2 to 3 hours to allow the Matrigel to solidify. The color images of the Transwell membranes were captured by bright-field microscopy (M165 FC, Leica, Germany), and all the migrated or invaded cells from each Transwell membrane were counted. At least two Transwell chambers were used in each assay, and all the Transwell assays were repeated at least three times. The average numbers of migrated or invaded cells are presented in the results.

Cell adhesion assay

HUVECs (2×10^4) were seeded in each well of a 96-well plate and cultured for 24 hours to form a confluent monolayer. Afterward, 100 μl of cell suspension containing 1×10^4 MCF7-C3, M-SSP6, A549-C3, or A-SSP6 cells was added on top of the HUVEC monolayer and incubated at 37°C for 30 min. Nonattached cells were washed away with phosphate-buffered saline (PBS) twice, and fresh medium was added to each well of the same culture plate. The green fluorescent images of the attached cells were taken by fluorescence microscopy (Carl Zeiss), and at least five images were used for quantification.

Colony formation assay

Two milliliters of cell suspension containing 2×10^3 (MCF7-C3 or M-SSP6) or 1×10^3 (A549-C3 or A-SSP6) cells was seeded in each well of the six-well plates and then cultured for 10 days. The colonies were fixed with 4% PFA for 15 min and stained with 0.5% crystal violet for another 15 min. Stained colonies with more than 50 cells per colony were counted. The results were calculated as the numbers of stained colonies per well.

Blood collection, CTC analysis, and experimental lung colonization model

Female NOD/SCID mice aged 6 to 8 weeks were used and maintained in the Animal Facility of the University of Macau. All animal experiments were approved by The Animal Research Ethics Committee of the University of Macau. Before the injection, cells were collected by trypsinization and washed with PBS twice and kept on ice. After measurement of cell density, 2×10^6 cells were intravenously injected into the blood circulation of each mouse through tail vein injection. After 4 or 6 hours, 750 μl of fresh whole blood was collected via cardiac puncture using a 27-gauge needle connected to a 1-ml syringe prefilled with 100 μl of PBS containing 10 mM EDTA. Blood smears were prepared from each mouse by pipetting 5 μl of blood onto a glass slide and sliding them into a thin layer of the blood. Then, cells in the monolayer area of the slide were imaged by fluorescence microscopy (Carl Zeiss). For in situ observation of CTCs in the blood samples, red blood cells were removed using lysis buffer, and the rest of the blood samples were transferred into a confocal dish for live-cell imaging by fluorescence microscopy (Carl Zeiss).

For the lung metastasis experiment, 1×10^6 cells were intravenously injected into the tail vein of the mice, and the mice were euthanized at different time points after the injection. The lung tissues were dissected to detect lung metastatic foci under a fluorescent stereomicroscope (M165 FC, Leica) using GFP filters. Then, the lung tissues were fixed with 4% PFA for 48 hours. Afterward, the tissues were washed with PBS, embedded in paraffin (Leica Biosystems), sectioned at 5 μm in thickness using a microtone (Leica Biosystems), and stained by hematoxylin and eosin (H&E) (Leica Biosystems). Last, the images of the H&E-stained lung tissues were taken by an Aperio Scanner System (Leica) at a magnification of ×20.

Orthotopic lung xenografts in NOD/SCID mice and CTCs analyses

The method of the in vivo spontaneous lung cancer metastasis model was designed according to Ross's description (*75*). A549-C3 and A-SSP6 cells were trypsinized and suspended in PBS and then mixed with Matrigel matrix (#354234, Corning, USA) at a ratio of 1:1 to achieve a final concentration of 1.0×10^5/μl. This cell suspension was kept on ice until injection. For orthotopic injection, 6- to 8-week-old female NOD/SCID mice were anesthetized with avertin (#T4840-2, Sigma-Aldrich, USA). A 0.8-cm surgical incision was made along the posterior medial line of the right thorax, and then, the fascia and adipose tissue layer were dissected and retracted to expose the lateral ribs, the intercostal space, and the right lung parenchyma. Upon confirmation of the right lung respiratory variation, 3 million suspended cells were injected into the lung tissue by a 30-gauge hypodermic needle. The needle was rapidly withdrawn, and the mice were observed for the possibility of a pneumothorax. Wound suture clips were used to seal the primary wound in the fascia and skin layers. The mice were observed after procedure for 3 to 4 hours, and their body weights and wound healing were monitored weekly. In addition, for the CTCs or CTC clusters analysis in this model, the blood samples were collected every week for 4 weeks after implantation, and the number of single CTCs or CTC clusters was quantified. Moreover, the blood vessels of animals were also examined to count the number of CTCs remained in blood circulation by fluorescence microscopy.

RNA-seq and data analysis

MCF7-C3 and M-SSP6 cells were collected and dissolved with TRIzol (#15596026, Thermo Fisher Scientific, USA). Samples were sent to Novogene (Tianjin, China) for RNA extraction (RNA integrity number, >9.0), purification, library preparation, sequencing, and basic data analysis. A $P < 0.05$ and a fold change of ≥ 1.5 were used as the thresholds to identify the differentially expressed genes with statistical significance.

RNA extraction and qRT-PCR

Total RNA was extracted using TRIzol reagent, and reverse transcription reactions were performed with an iScript cDNA synthesis kit (#1778890, Bio-Rad, USA). The relative levels of gene transcripts compared with that of the control gene [glyceraldehyde-3-phosphate dehydrogenase (GAPDH)] were determined by iTaq Universal SYBR Green (#1725122, Bio-Rad, USA). The qRT-PCR primers are listed in table S1.

Western blotting

Briefly, cell lysates were prepared in radioimmunoprecipitation assay buffer (150 mM NaCl, 50 mM tris-HCl, 0.5% SDS, and 1% Triton X-100) supplemented with 1% protease and 1% phosphatase inhibitor cocktail (Sigma-Aldrich). Proteins were separated by SDS–polyacrylamide gel electrophoresis and transferred to a nitrocellulose membrane (Bio-Rad). The membrane was blocked with 5% Blotting-Grade Blocker (#1706404, Bio-Rad, USA) in 1× tris-buffered saline with 0.2% Tween 20 (TBST) for 1 hour and then incubated with specific primary antibodies at 4°C overnight. Primary antibodies against VIM (#5741), PG (#2309), ITGB1 (#9699), FAK (#3285), p-Src (#6943), Src (#2109), CLDN1 (#13995), ZO-1 (#13663), ZEB1 (#3396), p-AKT (#4060), AKT (#4685), p-ERK1/2 (#4370), ERK1/2 (#4695), Bcl-2 (#15071) and GAPDH (#2118) were obtained from Cell Signaling Technology (1:2000). Antibodies against PKP1 (ab183512), CDH1 (ab1416), β-catenin (ab32572), and FN1 (ab2413) were obtained from Abcam (1:2000). Anti-DSC2 antibody (#326200) was purchased from Invitrogen (1:1000). After three washes with TBST, the protein blot was incubated with species-specific secondary antibody at room temperature for 1 hour. Last, the proteins were visualized using the Clarity Western ECL Substrate (#1705061, Bio-Rad, USA) and imaged by the ChemiDoc Touch Imaging System (Bio-Rad).

siRNA transfection and lentivirus infection

Two different siRNA duplexes of CDH1, VIM, and FN1 were designed and purchased from Ambion. RNAiMAX (Invitrogen) was used. Each specific siRNA was premixed with serum-free medium and incubated for 20 min. The siRNA mixtures were added to the cells and incubated for 48 hours, after which their silencing effects were determined by qRT-PCR and Western blotting. The siRNA sequences are listed in table S2.

The human shRNA vectors targeting DSC2, PKP1, VIM, FN1, and ZEB1 (targeting sequences are shown in table S2); CRISPR-Cas9–mediated knockout of ITGB1 (targeting sequences are shown in table S2); and the overexpression vectors (DSC2, VIM, and ZEB1; targeting sequences are shown in table S3) were purchased from VectorBuilder Company. The targeting plasmid, packaging plasmids of vesicular stomatitis virus glycoprotein, and dR8.2 were mixed in DMEM without FBS at weight ratios of 3:1:2. Afterward, the mixture and polyethylenimine were added to cultured 293 T cells

(generally 90% confluence) to produce lentiviruses. The viral supernatants were collected after 48 to 72 hours of transfection and stored at −80°C. Cancer cells were infected with viral supernatants for 72 hours and then selected with puromycin (2 μg/ml; #P8833, Sigma-Aldrich, Germany) for stably infected cell lines.

IF staining

Cells were seeded onto sterilized glass coverslips in 35-mm culture dishes and cultured for the designated time periods. For the suspended cells, the coverslips were precoated with poly-D-lysine hydrobromide (#P7866, Sigma-Aldrich, USA) to make cells attach within 30 min. The cells were fixed with 4% PFA and permeabilized with 0.2% Triton X-100 (#T8787, Sigma-Aldrich, Germany) at room temperature. After blocking with 3% bovine serum albumin for 1 hour, the cells were incubated with primary antibodies at 4°C overnight and with Alexa fluorescent–conjugated secondary antibodies (Invitrogen) at room temperature for 1 hour. Last, the cells were counterstained with Hoechst 33342 (#H3570, Thermo Fisher Scientific, USA) and imaged by fluorescence confocal microscopy (Carl Zeiss LSM710).

Immunohistochemistry

Tissue microarray slides were purchased from Superchip Company (Shanghai, China). IHC was performed using the IHC Detection Kit (Abcam, ab64264) according to the manufacturer's instructions. Paraffin-embedded tissue sections were deparaffinized, rehydrated, subjected to antigen retrieval, permeabilized, blocked, and incubated with primary antibodies against DSC2 (Invitrogen), PKP1 (Abcam), VIM (Cell Signaling Technology), and ZEB1 (Sigma-Aldrich) at 4°C overnight. Biotinylated secondary antibody was incubated for 30 min, and the antigen-antibody interaction was revealed with the streptavidin-biotin–horseradish peroxidase system using diaminobenzidine as a chromogen. Nuclei were counterstained with hematoxylin (Sigma-Aldrich). Images were obtained with an Aperio Scanner System (Leica) at a magnification of ×20. The expression levels of DSC2, PKP1, VIM, and ZEB1 were determined by semiquantitative analysis. IHC scores were graded according to percentage of stained cells as described (*57*). The percentage scores were assigned as follows: 0, none; 1, <1% of positively staining cells; 2, 1 to 10%; 3, 11 to 33%; 4, 34 to 66%; and 67 to 100%.

Statistical analysis

All data are expressed as the means ± SD from at least three independent experiments. One-way analysis of variance (ANOVA), two-way ANOVA, or Student's *t* test was used for statistically significant analysis, and $^{*}P < 0.05$, $^{**}P < 0.01$, $^{***}P < 0.001$, and $^{****}P < 0.0001$ were considered to be statistically significant compared with the relative control group.

SUPPLEMENTARY MATERIALS

Supplementary material for this article is available at https://science.org/doi/10.1126/sciadv.abg7265

View/request a protocol for this paper from *Bio-protocol*.

REFERENCES AND NOTES

1. G. P. Gupta, J. Massagué, Cancer metastasis: Building a framework. *Cell* **127**, 679–695 (2006).
2. N. Bednarz-Knoll, C. Alix-Panabières, K. Pantel, Plasticity of disseminating cancer cells in patients with epithelial malignancies. *Cancer Metastasis Rev.* **31**, 673–687 (2012).
3. K. J. Luzzi, I. C. MacDonald, E. E. Schmidt, N. Kerkvliet, V. L. Morris, A. F. Chambers, A. C. Groom, Multistep nature of metastatic inefficiency: Dormancy of solitary cells after successful extravasation and limited survival of early micrometastases. *Am. J. Pathol.* **153**, 865–873 (1998).
4. A. F. Chambers, A. C. Groom, I. C. MacDonald, Dissemination and growth of cancer cells in metastatic sites. *Nat. Rev. Cancer* **2**, 563–572 (2002).
5. J. Massagué, A. C. Obenauf, Metastatic colonization by circulating tumour cells. *Nature* **529**, 298–306 (2016).
6. I. J. Fidler, M. L. Kripke, Metastasis results from preexisting variant cells within a malignant tumor. *Science* **197**, 893–895 (1977).
7. E. Racila, D. Euhus, A. J. Weiss, C. Rao, J. McConnell, L. W. M. M. Terstappen, J. W. Uhr, Detection and characterization of carcinoma cells in the blood. *Proc. Natl. Acad. Sci. U.S.A.* **95**, 4589–4594 (1998).
8. L. A. Liotta, E. Kohn, Cancer and the homeless cell. *Nature* **430**, 973–974 (2004).
9. P. Mehlen, A. Puisieux, Metastasis: A question of life or death. *Nat. Rev. Cancer* **6**, 449–458 (2006).
10. J. M. Barnes, J. T. Nauseef, M. D. Henry, Resistance to fluid shear stress is a conserved biophysical property of malignant cells. *PLOS ONE* **7**, e50973 (2012).
11. D. Wirtz, K. Konstantopoulos, P. C. Searson, The physics of cancer: The role of physical interactions and mechanical forces in metastasis. *Nat. Rev. Cancer* **11**, 512–522 (2011).
12. V. T. Turitto, Blood viscosity, mass transport, and thrombogenesis. *Prog. Hemost. Thromb.* **6**, 139–177 (1982).
13. Q. Huang, X. Hu, W. He, Y. Zhao, S. Hao, Q. Wu, S. Li, S. Zhang, M. Shi, Fluid shear stress and tumor metastasis. *Am. J. Cancer Res.* **8**, 763–777 (2018).
14. M. J. Mitchell, M. R. King, Fluid shear stress sensitizes cancer cells to receptor-mediated apoptosis via trimeric death receptors. *New J. Phys.* **15**, 015008 (2013).
15. A. Fu, S. Ma, N. Wei, B. X. Xuan Tan, E. Y. Tan, K. Q. Luo, High expression of MnSOD promotes survival of circulating breast cancer cells and increases their resistance to doxorubicin. *Oncotarget* **7**, 50239–50257 (2016).
16. H. J. Lee, M. F. Diaz, K. M. Price, J. A. Ozuna, S. Zhang, E. M. Sevick-Muraca, J. P. Hagan, P. L. Wenzel, Fluid shear stress activates YAP1 to promote cancer cell motility. *Nat. Commun.* **8**, 14122 (2017).
17. S. Regmi, A. Fu, K. Q. Luo, High shear stresses under exercise condition destroy circulating tumor cells in a microfluidic system. *Sci. Rep.* **7**, 39975 (2017).
18. Y. Xin, K. Li, M. Yang, Y. Tan, Fluid shear stress induces EMT of circulating tumor cells via JNK signaling in favor of their survival during hematogenous dissemination. *Int. J. Mol. Sci.* **21**, 8115 (2020).
19. N. Ortiz-Otero, J. R. Marshall, B. W. Lash, M. R. King, Platelet mediated TRAIL delivery for efficiently targeting circulating tumor cells. *Nanoscale Adv.* **2**, 3942–3953 (2020).
20. I. J. Fidler, The pathogenesis of cancer metastasis: The 'seed and soil' hypothesis revisited. *Nat. Rev. Cancer* **3**, 453–458 (2003).
21. T. G. Papaioannou, C. Stefanadis, Vascular wall shear stress: Basic principles and methods. *Hell. J. Cardiol.* **46**, 9–15 (2005).
22. M.-E. Francart, J. Lambert, A. M. Vanwynsberghe, E. W. Thompson, M. Bourcy, M. Polette, C. Gilles, Epithelial-mesenchymal plasticity and circulating tumor cells: Travel companions to metastases. *Dev. Dyn.* **3**, 432–450 (2018).
23. B. Aktas, M. Tewes, T. Fehm, S. Hauch, R. Kimmig, S. Kasimir-Bauer, Stem cell and epithelial-mesenchymal transition markers are frequently overexpressed in circulating tumor cells of metastatic breast cancer patients. *Breast Cancer Res.* **11**, R46 (2009).
24. S. Kasimir-Bauer, O. Hoffmann, D. Wallwiener, R. Kimmig, T. Fehm, Expression of stem cell and epithelial-mesenchymal transition markers in primary breast cancer patients with circulating tumor cells. *Breast Cancer Res.* **14**, R15 (2012).
25. A. Hanssen, J. Wagner, T. M. Gorges, A. Taenzer, F. G. Uzunoglu, C. Driemel, N. H. Stoecklein, W. T. Knoefel, S. Angenendt, S. Hauch, D. Atanackovic, S. Loges, S. Riethdorf, K. Pantel, H. Wikman, Characterization of different CTC subpopulations in non-small cell lung cancer. *Sci. Rep.* **6**, 28010 (2016).
26. M. J. Mitchell, C. Denais, M. F. Chan, Z. Wang, J. Lammerding, M. R. King, Lamin A/C deficiency reduces circulating tumor cell resistance to fluid shear stress. *Am J. Physiol.-Cell* **309**, C736–C746 (2015).
27. A. Woroniuk, A. Porter, G. White, D. T. Newman, Z. Diamantopoulou, T. Waring, C. Rooney, D. Strathdee, D. J. Marston, K. M. Hahn, O. J. Sansom, T. Zech, A. Malliri, STEF/TIAM2-mediated Rac1 activity at the nuclear envelope regulates the perinuclear actin cap. *Nat. Commun.* **9**, 2124 (2018).
28. D. L. Moose, B. L. Krog, T.-H. Kim, L. Zhao, S. Williams-Perez, G. Burke, L. Rhodes, M. Vanneste, P. Breheny, M. Milhem, C. S. Stipp, A. C. Rowat, M. D. Henry, Cancer cells resist mechanical destruction in circulation via RhoA/Actomyosin-dependent Mechano-adaptation. *Cell Rep.* **30**, 3864–3874.e6 (2020).
29. I. J. Fidler, The relationship of embolic homogeneity, number, size and viability to the incidence of experimental metastasis. *Eur J. Cancer.* **9**, 223–227 (1973).
30. M. Yu, A. Bardia, B. S. Wittner, S. L. Stott, M. E. Smas, D. T. Ting, S. J. Isakoff, J. C. Ciciliano, M. N. Wells, A. M. Shah, K. F. Concannon, M. C. Donaldson, L. V. Sequist, E. Brachtel, D. Sgroi, J. Baselga, S. Ramaswamy, M. Toner, D. A. Haber, S. Maheswaran, Circulating

breast tumor cells exhibit dynamic changes in epithelial and mesenchymal composition. *Science* **339**, 580–584 (2013).
31. Y. Zheng, D. T. Miyamoto, B. S. Wittner, J. P. Sullivan, N. Aceto, N. V. Jordan, M. Yu, N. M. Karabacak, V. Comaills, R. Morris, R. Desai, N. Desai, E. Emmons, J. D. Milner, R. J. Lee, C.-L. Wu, L. V. Sequist, W. Haas, D. T. Ting, M. Toner, S. Ramaswamy, S. Maheswaran, D. A. Haber, Expression of β-globin by cancer cells promotes cell survival during blood-borne dissemination. *Nat. Commun.* **8**, 14344 (2017).
32. M. Yu, S. Stott, M. Toner, S. Maheswaran, D. A. Haber, Circulating tumor cells: Approaches to isolation and characterization. *J. Cell Biol.* **192**, 373–382 (2011).
33. N. Aceto, A. Bardia, D. T. Miyamoto, M. C. Donaldson, B. S. Wittner, J. A. Spencer, M. Yu, A. Pely, A. Engstrom, H. Zhu, B. W. Brannigan, R. Kapur, S. L. Stott, T. Shioda, S. Ramaswamy, D. T. Ting, C. P. Lin, M. Toner, D. A. Haber, S. Maheswaran, Circulating tumor cell clusters are oligoclonal precursors of breast cancer metastasis. *Cell* **158**, 1110–1122 (2014).
34. X. Liu, R. Taftaf, M. Kawaguchi, Y. F. Chang, W. Chen, D. Entenberg, Y. Zhang, L. Gerratana, S. Huang, D. B. Patel, E. Tsui, V. Adorno-Cruz, S. M. Chirieleison, Y. Cao, A. S. Harney, S. Patel, A. Patsialou, Y. Shen, S. Avril, H. L. Gilmore, J. D. Lathia, D. W. Abbott, M. Cristofanilli, J. S. Condeelis, H. Liu, Homophilic CD44 interactions mediate tumor cell aggregation and polyclonal metastasis in patient-derived breast cancer models. *Cancer Discov.* **9**, 96–113 (2019).
35. D. H. Lee, M. Jang, J. K. Park, Rapid one-step purification of single-cells encapsulated in alginate microcapsules from oil to aqueous phase using a hydrophobic filter paper: Implications for single-cell experiments. *Biotechnol. J.* **9**, 1233–1240 (2014).
36. N. Cirillo, M. Lanza, A. de Rosa, M. Cammarota, A. la Gatta, F. Gombos, A. Lanza, The most widespread desmosomal cadherin, desmoglein 2, is a novel target of caspase 3-mediated apoptotic machinery. *J. Cell. Biochem.* **103**, 598–606 (2008).
37. C. A. Franzen, V. Todorović, B. V. Desai, S. Mirzoeva, X. J. Yang, K. J. Green, J. C. Pelling, The desmosomal armadillo protein plakoglobin regulates prostate cancer cell adhesion and motility through vitronectin-dependent Src signaling. *PLOS ONE* **7**, e42132 (2012).
38. M. Hatzfeld, R. Keil, T. M. Magin, Desmosomes and intermediate filaments: Their consequences for tissue mechanics. *CSH. Perspect. Biol.* **9**, a029157 (2017).
39. W.-K. Fang, L.-D. Liao, F.-M. Zeng, P.-X. Zhang, J.-Y. Wu, J. Shen, L.-Y. Xu, E.-M. Li, Desmocollin-2 affects the adhesive strength and cytoskeletal arrangement in esophageal squamous cell carcinoma cells. *Mol. Med. Rep.* **10**, 2358–2364 (2014).
40. L. Saias, A. Gomes, M. Cazales, B. Ducommun, V. Lobjois, Cell–cell adhesion and cytoskeleton tension oppose each other in regulating tumor cell aggregation. *Cancer Res.* **75**, 2426–2433 (2015).
41. F. Gava, B. Ducommum, V. Lobjois, Anchorage-independent tumor cells clustering and implication in metastatic dissemination. *Cancer Therapy. Oncol. Int. J.* **6**, 555683 (2017).
42. K. J. Cheung, V. Padmanaban, V. Silvestri, K. Schipper, J. D. Cohen, A. N. Fairchild, M. A. Gorin, J. E. Verdone, K. J. Pienta, J. S. Bader, A. J. Ewald, Polyclonal breast cancer metastases arise from collective dissemination of keratin 14-expressing tumor cell clusters. *Proc. Natl. Acad. Sci. U.S.A.* **113**, E854–E863 (2016).
43. K. S. M. Smalley, P. Brafford, N. K. Haass, J. M. Brandner, E. Brown, M. Herlyn, Up-regulated expression of zonula occludens protein-1 in human melanoma associates with N-cadherin and contributes to invasion and adhesion. *Am. J. Pathol.* **166**, 1541–1554 (2005).
44. A. J. Ewald, A. Brenot, M. Duong, B. S. Chan, Z. Werb, Collective epithelial migration and cell rearrangements drive mammary branching morphogenesis. *Dev. Cell* **14**, 570–581 (2008).
45. J. W. Choi, J. K. Kim, Y. J. Yang, P. Kim, K. H. Yoon, S. H. Yun, Urokinase exerts antimetastatic effects by dissociating clusters of circulating tumor cells. *Cancer Res.* **75**, 4474–4482 (2015).
46. K. J. Cheung, A. J. Ewald, A collective route to metastasis: Seeding by tumor cell clusters. *Science* **352**, 167–169 (2016).
47. C.-F. Li, J. Y. Chen, Y. H. Ho, W. H. Hsu, L. C. Wu, H. Y. Lan, D. S. S. Hsu, S. K. Tai, Y. C. Chang, M. H. Yang, Snail-induced claudin-11 prompts collective migration for tumour progression. *Nat. Cell Biol.* **21**, 251–262 (2019).
48. H. Yang, L. Guan, S. Li, Y. Jiang, N. Xiong, L. Li, C. Wu, H. Zeng, Y. Liu, Mechanosensitive caveolin-1 activation-induced PI3K/Akt/mTOR signaling pathway promotes breast cancer motility, invadopodia formation and metastasis in vivo. *Oncotarget* **7**, 16227–16247 (2016).
49. T. Hagihara, J. Kondo, H. Endo, M. Ohue, Y. Sakai, M. Inoue, Hydrodynamic stress stimulates growth of cell clusters via the ANXA1/PI3K/AKT axis in colorectal cancer. *Sci. Rep.* **9**, 20027 (2019).
50. Q. Huang, S. Li, X. Hu, M. Sun, Q. Wu, H. Dai, Y. Tan, F. Sun, C. Wang, X. Rong, W. Liao, J. Peng, J. Xiao, L. Huang, J. Wang, B. Liang, K. Lin, Y. Liu, M. Shi, Shear stress activates ATOH8 via autocrine VEGF promoting glycolysis dependent-survival of colorectal cancer cells in the circulation. *J. Exp. Clin. Cancer Res.* **39**, 25 (2020).
51. E. W. Howard, S. C. L. Leung, H. F. Yuen, C. W. Chua, D. T. Lee, K. W. Chan, X. Wang, Y. C. Wong, Decreased adhesiveness, resistance to anoikis and suppression of GRP94 are integral to the survival of circulating tumor cells in prostate cancer. *Clin. Exp. Metastasis* **25**, 497–508 (2008).
52. T. Landemaine, A. Jackson, A. Bellahcène, N. Rucci, S. Sin, B. M. Abad, A. Sierra, A. Boudinet, J. M. Guinebretière, E. Ricevuto, C. Noguès, M. Briffod, I. Bièche, P. Cherel, T. Garcia, V. Castronovo, A. Teti, R. Lidereau, K. Driouch, A six-gene signature predicting breast cancer lung metastasis. *Cancer Res.* **68**, 6092–6099 (2008).
53. K. Kolegraff, P. Nava, M. N. Helms, C. A. Parkos, A. Nusrat, Loss of desmocollin-2 confers a tumorigenic phenotype to colonic epithelial cells through activation of Akt/β-catenin signaling. *Mol. Biol. Cell* **22**, 1121–1134 (2011).
54. R. Sanz-Pamplona, J. García-García, S. Franco, X. Messeguer, K. Driouch, B. Oliva, À. Sierra, A taxonomy of organ-specific breast cancer metastases based on a protein–protein interaction network. *Mol. BioSyst.* **8**, 2085–2096 (2012).
55. D. Haase, T. Cui, L. Yang, Y. Ma, H. Liu, B. Theis, I. Petersen, Y. Chen, Plakophilin 1 is methylated and has a tumor suppressive activity in human lung cancer. *Exp. Mol. Pathol.* **108**, 73–79 (2019).
56. J. Martin-Padron, L. Boyero, M. I. Rodriguez, A. Andrades, I. Díaz-Cano, P. Peinado, C. Baliñas-Gavira, J. C. Alvarez-Perez, I. F. Coira, M. E. Fárez-Vidal, P. P. Medina, Plakophilin 1 enhances MYC translation, promoting squamous cell lung cancer. *Oncogene* **39**, 5479–5493 (2020).
57. F. B. Fromowitz, M. V. Viola, S. Chao, S. Oravez, Y. Mishriki, G. Finkel, R. Grimson, J. Lundy, ras p21 expression in the progression of breast cancer. *Hum. Pathol.* **18**, 1268–1275 (1987).
58. A. N. May, B. D. Crawford, A. M. Nedelcu, In vitro model-systems to understand the biology and clinical significance of circulating tumor cell clusters. *Front. Oncol.* **8**, 63 (2018).
59. M. Bourcy, M. Suarez-Carmona, J. Lambert, M. E. Francart, H. Schroeder, C. Delierneux, N. Skrypek, E. W. Thompson, G. Jérusalem, G. Berx, M. Thiry, S. Blacher, B. G. Hollier, A. Noël, C. Oury, M. Polette, C. Gilles, Tissue factor induced by epithelial-mesenchymal transition triggers a procoagulant state that drives metastasis of circulating tumor cells. *Cancer Res.* **76**, 4270–4282 (2016).
60. A. D. Grigore, M. K. Jolly, D. Jia, M. C. Farach-Carson, H. Levine, Tumor budding: The name is EMT. Partial EMT. *J. Clin. Med.* **5**, 51 (2016).
61. A. J. Armstrong, M. S. Marengo, S. Oltean, G. Kemeny, R. L. Bitting, J. D. Turnbull, C. I. Herold, P. K. Marcom, D. J. George, M. A. Garcia-Blanco, Circulating tumor cells from patients with advanced prostate and breast cancer display both epithelial and mesenchymal markers. *Mol. Cancer Res.* **9**, 997–1007 (2011).
62. M. K. Jolly, J. A. Somarelli, M. Sheth, A. Biddle, S. C. Tripathi, A. J. Armstrong, S. M. Hanash, S. A. Bapat, A. Rangarajan, H. Levine, Hybrid epithelial/mesenchymal phenotypes promote metastasis and therapy resistance across carcinomas. *Pharmacol. Therapeut.* **194**, 161–184 (2019).
63. X. Zhang, L. Yang, S. Chien, Y. Lv, Suspension state promotes metastasis of breast cancer cells by up-regulating cyclooxygenase-2. *Theranostics* **8**, 3722–3736 (2018).
64. R.-r. Wei, D. N. Sun, H. Yang, J. Yan, X. Zhang, X. L. Zheng, X. H. Fu, M. Y. Geng, X. Huang, J. Ding, CTC clusters induced by heparanase enhance breast cancer metastasis. *Acta Pharmacol. Sin.* **39**, 1326–1337 (2018).
65. V. Thamilselvan, A. Patel, J. van der Voort van Zyp, M. D. Basson, Colon cancer cell adhesion in response to Src kinase activation and actin-cytoskeleton by non-laminar shear stress. *J. Cell. Biochem.* **92**, 361–371 (2004).
66. K. Egan, N. Cooke, D. Kenny, Living in shear: Platelets protect cancer cells from shear induced damage. *Clin. Exp. Metastasis* **31**, 697–704 (2014).
67. K. Tang, S. Li, P. Li, Q. Xia, R. Yang, T. Li, L. Li, Y. Jiang, X. Qin, H. Yang, C. Wu, F. You, Y. Tan, Y. Liu, Shear stress stimulates integrin β1 trafficking and increases directional migration of cancer cells via promoting deacetylation of microtubules. *BBA Mol. Cell. Res.* **1867**, 118676 (2020).
68. R. Fan, T. Emery, Y. Zhang, Y. Xia, J. Sun, J. Wan, Circulatory shear flow alters the viability and proliferation of circulating colon cancer cells. *Sci. Rep.* **6**, 27073 (2016).
69. Y. Xin, X. Chen, X. Tang, K. Li, M. Yang, W. C. S. Tai, Y. Liu, Y. Tan, Mechanics and actomyosin-dependent survival/chemoresistance of suspended tumor cells in shear flow. *Biophys. J.* **116**, 1803–1814 (2019).
70. M. Saini, B. M. Szczerba, N. Aceto, Circulating tumor cell-neutrophil tango along the metastatic process. *Cancer Res.* **79**, 6067–6073 (2019).
71. K. Nakamura, M. J. Smyth, Immunoediting of cancer metastasis by NK cells. *Nat. Can.* **1**, 670–671 (2020).
72. J. Yan, G. Kloecker, C. Fleming, M. Bousamra II, R. Hansen, X. Hu, C. Ding, Y. Cai, D. Xiang, H. Donninger, J. W. Eaton, G. J. Clark, Human polymorphonuclear neutrophils specifically recognize and kill cancerous cells. *Onco. Targets. Ther.* **3**, e950163 (2014).
73. K. Q. Luo, V. C. Yu, Y. Pu, D. C. Chang, Application of the fluorescence resonance energy transfer method for studying the dynamics of caspase-3 activation during UV-induced apoptosis in living HeLa cells. *Biochem. Biophys. Res.* **283**, 1054–1060 (2001).

74. S. Ma, A. Fu, G. G. Y. Chiew, K. Q. Luo, Hemodynamic shear stress stimulates migration and extravasation of tumor cells by elevating cellular oxidative level. *Cancer Lett.* **388**, 239–248 (2017).
75. R. A. Okimoto, F. Breitenbuecher, V. R. Olivas, W. Wu, B. Gini, M. Hofree, S. Asthana, G. Hrustanovic, J. Flanagan, A. Tulpule, C. M. Blakely, H. J. Haringsma, A. D. Simmons, K. Gowen, J. Suh, V. A. Miller, S. Ali, M. Schuler, T. G. Bivona, Inactivation of Capicua drives cancer metastasis. *Nat. Genet.* **49**, 87–96 (2017).

Acknowledgments: We are grateful to H. Jia of K.Q.L.'s group for valuable discussions and technical assistance with the imaging. We would like to thank the Animal Facility, the Histology Core and Imaging Core Facilities of the Faculty of Health Sciences of the University of Macau. **Funding:** This work was supported by the Multi-Year Research Grant (MYRG2018-00092-FHS) and the Frontiers Science Center (FSC-2021) of the University of Macau. **Author contributions:** K.L. and K.Q.L. designed the research studies. K.L. M.Z., and H.T. conducted experiments. K.L. K.Q.L., and R.W. analyzed the data. K.Q.L. and K.L. wrote the manuscript. **Competing interests:** The authors declare that they have no competing interests. **Data and materials availability:** All data needed to evaluate the conclusions in the paper are present in the paper and/or the Supplementary Materials.

Submitted 24 January 2021
Accepted 9 August 2021
Published 29 September 2021
10.1126/sciadv.abg7265

Citation: K. Li, R. Wu, M. Zhou, H. Tong, K. Q. Luo, Desmosomal proteins of DSC2 and PKP1 promote cancer cells survival and metastasis by increasing cluster formation in circulatory system. *Sci. Adv.* **7**, eabg7265 (2021).